JGR Oceans

RESEARCH ARTICLE
10.1029/2022JC019002

A Simulation of Snow on Antarctic Sea Ice Based on Satellite Data and Climate Reanalyses

Isobel R. Lawrence[1], Andrew L. Ridout[2], Andrew Shepherd[3], and Rachel Tilling[4]

[1]ESA ESRIN, Frascati, Italy, [2]Centre for Polar Observation and Modelling, University College London, London, UK, [3]Centre for Polar Observation and Modelling, University of Northumbria, Newcastle, UK, [4]NASA Goddard Space Flight Center, Greenbelt, MD, USA

Abstract Although snow plays an important role in the energy and mass balance of sea ice, it is little studied in the Southern Ocean. We present a Lagrangian model of snow on sea ice, CASSIS, that simulates the daily creation and drift of floes. Drifting floes accumulate snow from the atmosphere and the Antarctic ice sheet, and lose snow to the ocean and snow-ice formation. The depth of snow on Southern Ocean sea ice increases in all sectors between autumn and spring 1981–2021, reaching 40 cm in much of the Weddell Sea, coastal Amundsen Sea and south east Indian Ocean. The root mean square difference between seasonally-averaged model and ship-based snow depths is 13.1 cm, and between modeled and airborne snow depths from Operation IceBridge is 13.5 cm. Our model offers an alternative long-term snow depth record to that from passive microwave (PM) radiometry, which does not capture the seasonal growth of the snow cover. We find that although the average circumpolar snow layer thickness has increased by 16 mm between 1981 and 2021 ($P = 0.004$), there has been a decrease of 13 mm in the Southern Pacific Ocean ($P = 0.133$, but significant in spring and autumn), driven by a reduction of summer sea ice extent in this region. Our model paves the way for improved satellite-based estimates of Antarctic sea ice thickness.

Plain Language Summary Knowing the thickness of the snow layer that blankets sea ice is important for climate studies, and it is essential for estimating the thickness and volume of sea ice from satellites. Here we present a model which simulates the snow cover on Antarctic sea ice using information about sea ice motion, snowfall, wind redistribution and snowpack processes. Our modeled snow depths are a good alternative to the existing long-term records from PM satellites, which don't properly capture the seasonal growth of the snow cover. We analyze trends in snow depth over the 41 years for which the model is run, and find that while the snow cover of Antarctic sea ice has increased overall, it has decreased in the South Pacific Ocean because of changes in the amount of sea ice left in this region at the end of the summer melt season.

Key Points:

- Our model, CASSIS, simulates the daily drift of sea ice floes in the Southern Ocean and the evolution of their snow cover
- Modeled snow depth increases in all sectors of the Southern Ocean between autumn and spring
- A reduction of snow depth in the South Pacific between 1981 and 2021 is a result of reduced late-summer sea ice concentration

Supporting Information:

Supporting Information may be found in the online version of this article.

Correspondence to:

I. R. Lawrence,
isobel.lawrence@esa.int

Citation:

Lawrence, I. R., Ridout, A. L., Shepherd, A., & Tilling, R. (2024). A simulation of snow on Antarctic sea ice based on satellite data and climate reanalyses. *Journal of Geophysical Research: Oceans*, *129*, e2022JC019002. https://doi.org/10.1029/2022JC019002

Received 21 JUN 2022
Accepted 19 NOV 2023

Author Contributions:

Conceptualization: Isobel R. Lawrence, Andrew L. Ridout, Andrew Shepherd, Rachel Tilling
Formal analysis: Isobel R. Lawrence, Andrew L. Ridout, Andrew Shepherd
Funding acquisition: Andrew Shepherd
Investigation: Isobel R. Lawrence, Andrew L. Ridout, Andrew Shepherd
Methodology: Isobel R. Lawrence, Andrew L. Ridout, Andrew Shepherd, Rachel Tilling
Software: Andrew L. Ridout
Supervision: Isobel R. Lawrence, Andrew Shepherd
Writing – original draft: Isobel R. Lawrence

1. Introduction

Snow is an important component of the climate system and a major source of freshwater to the ocean. For much of the year, snowfall over the Southern Ocean is intercepted by sea ice, which shrinks in extent annually from around 20 million square kilometers in September to typically less than 3 million square kilometers by the end of Austral summer (NSIDC, 2021). Snow insulates sea ice from the atmosphere, limiting thermodynamic growth and melt, and increases the albedo of the ice-covered ocean. It is also a key component of the sea ice mass balance, and snow depth estimates are essential for deriving sea ice thickness from satellite altimetry (Giles et al., 2007). Although the Antarctic continent is considered the largest desert on Earth, the Southern Ocean, which covers around 15% of the Earth's surface (Huang et al., 2016), receives more snowfall than anywhere else in the world (Figure 1). It snows there all year with little seasonality, owing to the persistent circumpolar baroclinic zone and the year-round availability of moisture from the ice-free ocean further north (Sodemann & Stohl, 2009).

Much of our knowledge of Antarctic sea ice has come from ship-based surveys conducted in the 1980s and 1990s which described a snowpack that was thicker, more heterogeneous, and older than that of the Arctic (Massom et al., 2001). Ice core analyses revealed a portion of the sea ice that was meteoric in origin, formed from the flooding and freezing of the snow cover. This snow-ice, little documented in the northern hemisphere (though likely existing in the Atlantic sector (Merkouriadi et al., 2017)), is prolific in the Southern Ocean, reportedly occurring in all regions and throughout the year (Massom et al., 2001). Another sea ice feature unique to the southern hemisphere is the accumulation of snow blown off the Antarctic continent. Due to the extreme slopes

Writing – review & editing: Isobel R. Lawrence

of the Antarctic ice sheet, pressure gradients cause strong, persistent winds to blow downhill towards the ocean, carrying snow with them (Fedotov et al., 1998). Strong enough to strip the sea ice in the first few km offshore of all its snow, katabatic winds typically die off some tens of km from the coast, where they deposit the redistributed snow (Bromwich & Kurtz, 1984; Fedotov et al., 1998).

Snow depth has been estimated from passive microwave (PM) satellites since the 1990s. The first of these products was derived from the Special Sensor Microwave/Imager (SSM/I) on board the United States Air Force Defense Meteorological Satellite Program Block 5D-2 satellites, and data spanning 1992–2007 are available from the NASA Goddard Space Flight Centre (GSFC). The methodology was subsequently applied to data from the Advanced Microwave Scanning Radiometer (AMSR) instruments aboard the AQUA satellite (2002–2011) (Comiso et al., 2003), and the GCOM-W1 satellite, which launched in 2012 and is still operational today. The methodology—based on the linear relationship between spectral gradient ratios and in-situ snow depths—works only for dry snow and is highly sensitive to melt events (Comiso et al., 2003), which are occurring with increasing frequency in the Antarctic (Boisvert et al., 2020). Further, due to the penetration depth at the frequencies utilized by the instrument, snow thickness resolution is limited to a maximum of 50 cm. In-situ records and buoy measurements report snow depths often in excess of 1 m on Southern Ocean sea ice (Massom et al., 2001; Nicolaus et al., 2016). The method is also sensitive to snow grain size, but since this is not measured routinely in the Southern Ocean, this sensitivity cannot be further explored. Despite these limitations, snow depths from SSM/I were found to agree well with ship-based observations between 1986 and 1995 (correlation = 0.81, Markus & Cavalieri, 1998), and the PM data sets provide the only multi-decadal observational record of snow on Southern Ocean sea ice to date.

In recent years, dual-frequency satellite altimetry has been used to derive snow depths on sea ice in both polar oceans (Garnier et al., 2021; Guerreiro et al., 2016; Kacimi & Kwok, 2020, 2022; Lawrence et al., 2018). While the approach shows promise, there are challenges in determining the depth of radar penetration into the snowpack and the ice freeboard, and in achieving compatibility between measurements acquired from sensors with markedly different spatial sampling (Fons et al., 2021; Giles et al., 2008; Willatt et al., 2010). Estimates using this approach are also limited in principle to the period between 2003 and 2008 (when the ICESat laser altimeter was operational) and in practice to after 2013 (when the AltiKa Ka-band altimeter was launched) and cannot therefore complement the complete record of Ku-band radar altimeter data acquired since the launch of ERS-1 in 1991. Estimates of snow depth that date back to the early 1990s and are independent of satellite altimetry are therefore desirable.

Efforts to model the Southern Ocean sea ice snow cover have been underway since the 1990s, however these have focused on the role of snow on sea ice and the wider climate (e.g., Fichefet & Maqueda, 1999; Holland et al., 2021; Powell et al., 2005), rather than estimating snow depth itself. The recent development of Arctic sea ice snow models (e.g., Blanchard-Wrigglesworth et al., 2018; Liston et al., 2020; Petty et al., 2018), which use snowfall data from atmospheric reanalysis combined with sea ice drift to simulate the evolution of the snowpack at daily resolution, have until now not been extended to the southern hemisphere. This is in part due to lack of in-situ observations, compounded by complex formation processes different from the Arctic, which are challenging to represent (Maksym et al., 2012).

Recent changes in Antarctic sea ice extent—including dramatic record-breaking lows in 2016 (Wang et al., 2019), 2017 (Turner et al., 2020) and 2022—suggest that Southern Ocean sea ice may be entering a period of decline after decades of increasing ice extent (Eayrs et al., 2021). However, a complete understanding of the drivers of this variability is lacking, in part due to the paucity of information on trends in the sea ice thickness which result largely from the lack of a long-term snow depth record.

Here we present the Centre for Polar Observation and Modelling (CPOM) Antarctic Snow on Sea Ice Simulation, CASSIS, a Lagrangian-network snow accumulation model forced with atmospheric reanalysis, satellite-derived sea ice concentration (SIC) and motion and initialized with ship-based observations from the SCAR Antarctic Sea Ice Processes and Climate (ASPeCt) data archive. The model accounts for snow blown onto sea ice from the Antarctic ice sheet, using output from the ice sheet mass balance model Regional Atmospheric Climate Model version 2 (RACMO2). Snow is lost to the ocean via a blowing-snow term which is a function of snow depth, wind speed and SIC and is calibrated with snow depths from ASPeCt. We include a fixed snow to snow-ice conversion ratio based on findings from field data, and explore the sensitivity of our snow depths estimates to this highly uncertain model parameter in Section 3.2. We undertake a comprehensive comparison of the regional/temporal

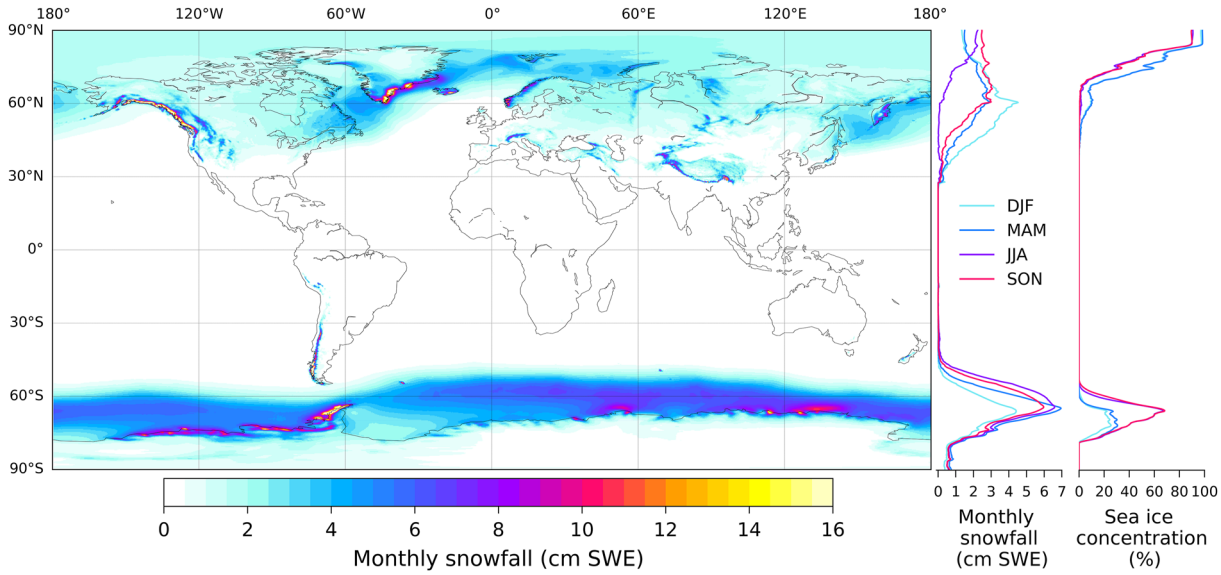

Figure 1. Average global snowfall (1979–2020) from ERA5 atmospheric reanalysis (Hersbach et al., 2023). Histograms show seasonal snowfall, and sea ice concentration from the NASA Goddard Space Flight Center (Cavalieri et al., 1996), with latitude.

variability of CASSIS snow depths with data from ships and aircraft, as well as snow depth estimates from PM radiometers SSM/I and AMSR(E/-2) (Section 3.3). We assess trends in the snow cover between 1981 and 2021 in Section 3.4, and discuss the seasonal growth of the snowpack and the model limitations in Section 4. In the following section we provide a summary of the data used for model input and validation, and describe the model algorithm.

2. Data and Methods

2.1. Model Input Data

2.1.1. Sea Ice Concentration

Daily SIC data (Cavalieri et al., 1996) are generated at the NASA GSFC and made available through the National Snow and Ice Data Center (NSIDC), provided on a Polar stereographic projection with tangential plane at 70°N/S, and a grid size of 25 km square. Sea ice concentration uncertainty is estimated as ±5% in winter and 15% in summer (NSIDC, 2003). In our model, snow accumulates daily where concentration ≧15%. If a Lagrangian point drifts into an area where SIC <15%, its snow cover is set to zero.

2.1.2. Sea Ice Motion Vectors

We use Polar Pathfinder daily sea ice motion vectors version 4 (Tschudi et al., 2019)—also available through NSIDC—to move the Lagrangian points of our model. The u and v vector components are provided on a 25 km EASE-Grid, calculated by optimally interpolating vectors derived from satellite (SMMR, SSM/I) microwave radiometry and Advanced Very High Resolution Radiometer visible imagery observations. Note that contrary to the information provided in the NSIDC data manual (at time of writing), the National Centers for Environmental Prediction reanalysis and buoy drift data are not utilized to derive motion vectors in the Southern Ocean (Tschudi et al., 2020). Sea ice motion vectors are supplied with a relative error which ranges between 0 and 100 and is a measure of the quality of the interpolated estimate. These can be used to weight estimates relative to each other, but are not applicable as quantitative error values (Walter N. Meier, personal communication, June 2023).

2.1.3. ERA5 Reanalysis Data: Snowfall, Temperature and Windspeed

The ERA5 reanalysis data set provides estimates of a variety of atmospheric, land and oceanic climate variables (Hersbach et al., 2023). Boisvert et al. (2020) assessed the performance of precipitation and snowfall in eight reanalysis products over the Southern Ocean, but conclude that a lack of robust in-situ data for comparison precludes an evaluation of which product is most accurate. However, ERA5 demonstrates similar snowfall magnitudes to MERRA2, with their differences being much less than the overall product spread, and the most

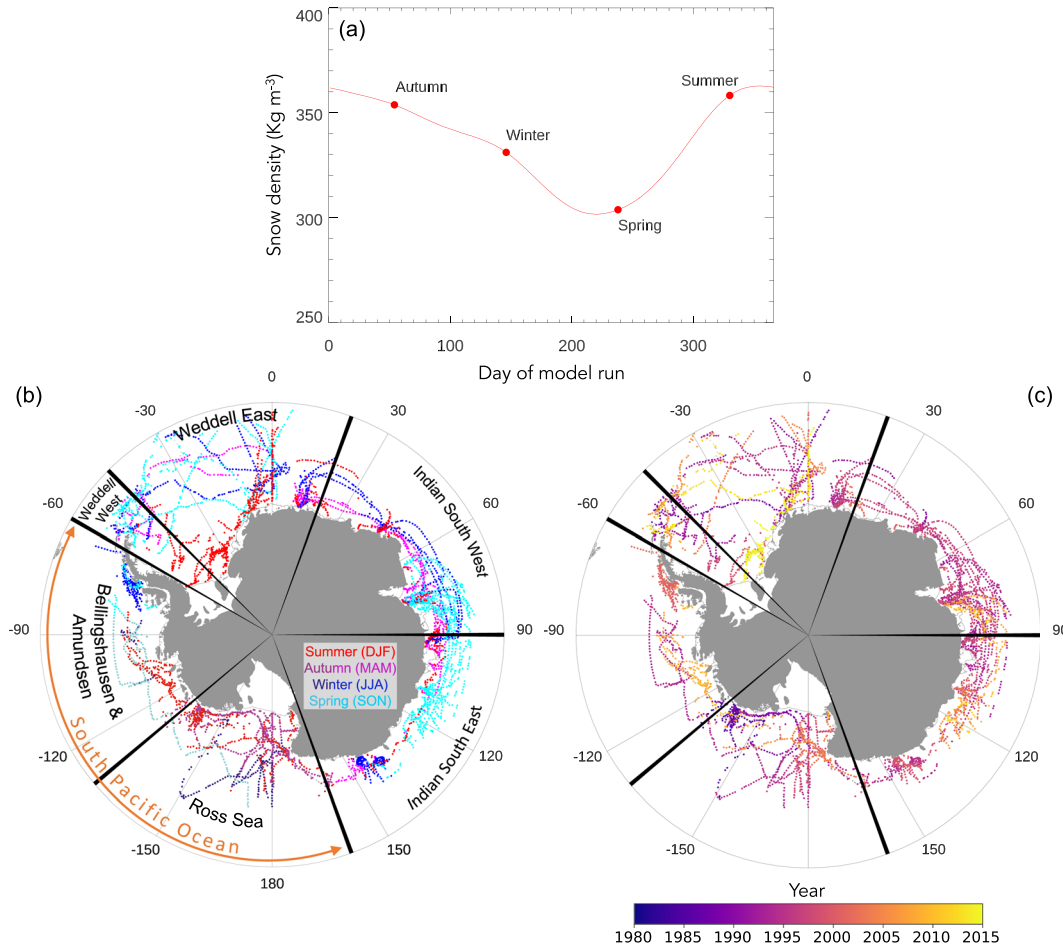

Figure 2. (a) Antarctic snow density function derived from in-situ data compiled in Massom et al. (2001). Snow densities were seasonally averaged using the number of snow pits as weighting, after Kurtz and Markus (2012). The four seasonal means were then interpolated using a Hamming tapered sinc function to estimate snow density as a function of day of model run, where day 0 = February 20th. Maps showing ASPeCt ship data for the years 1981–2016, colored by (b) season and (c) year.

similar spatial pattern of snowfall compared with data from the Cloudsat satellite. ERA5 has also been shown to offer improved estimates of surface temperature (Gossart et al., 2019) and windspeed (Dong et al., 2020) over the Ice sheet, compared with other reanalysis products. ERA5 variables are not provided with quantitative error estimates, though relative uncertainties based on the spread of ensemble members are available. These can help identify areas and periods where ERA5 is more, or less, reliable (ERA5 documentation, available at https://confluence.ecmwf.int/display/CKB/ERA5%3A+uncertainty+estimation, date of last access: 30 June 2023).

For our model we utilize 2 m air temperature, snowfall, and 10 m wind speed, all available on a 0.25° × 0.25° grid at hourly resolution. The "Snowfall" parameter, which represents the accumulated snowfall that falls to the Earth's surface, is the sum of the parameters "Large-scale snowfall" and "Convective snowfall," which are generated respectively by the cloud and convection schemes in the European Centre for Medium-Range Weather Forecasts Integrated Forecasting system. 2 m air temperature must be at or below 0°C for every hour of the day for snow to accumulate in our model. To estimate total daily snowfall, we sum hourly snowfall fields, which are provided in meters of snow water equivalent (SWE). SWE is converted to snow depth using a seasonally-varying density function (Figure 2a), derived from in-situ snow density measurements (Massom et al., 2001, Table 6). After Kurtz and Markus (2012), we seasonally averaged the snow densities using the number of snow pits as weighting. The four seasonal means were then interpolated using a Hamming tapered sinc function. We average the wind speeds every 6 hr (at midnight, 6 a.m., midday, and 6 p.m.) to estimate the amount of blown snow lost to the ocean four times a day (Section 2.3).

2.1.4. Katabatic Snow Fall

The RACMO2 calculates the individual components of Antarctic ice sheet surface mass balance, including precipitation and snow sublimation (van Wessem et al., 2018). Combining these processes with u and v wind speeds, the model outputs a term called "horizontal drifting snow transport," with units of kg m^{-1} s^{-1}, provided on a 27 × 27 km grid at daily resolution. This parameter represents, for each grid cell, the mass of snow traversing a 1-m-wide window (in the direction perpendicular to the wind direction), per second. Multiplying by the number of seconds in a day and the width of a grid-cell edge, we estimated the daily mass of snow leaving the Antarctic continent and being deposited over sea ice. We chose to redistribute the mass of snow by one RACMO2 grid pixel in the direction of the wind, equating to snow being carried by katabatic winds to a maximum distance of 38 km offshore (where wind direction is diagonal to grid axes). This, to first order, agrees with the limited reports regarding the distance at which katabatic winds lose momentum. Adolphs and Wendler (1995) remark that the strongest winds have been known to prevail up to 100 km offshore, but they typically die out some tens of kilometers into the ocean (Bromwich & Kurtz, 1984). We explored varying the distance over which snow is redistributed as a function of wind speed, but with typical katabatic snowfall values of less than 1 mm SWE per day, the term has a small influence on our model overall and so was not worth adjusting further.

2.1.5. Snow-Ice Formation

Excessive snow accumulation can depress sea ice floes below the ocean surface, causing flooding of basal snow layers (Massom et al., 2001). The subsequent freezing of flooded snow forms snow-ice, which is distinguishable from sea ice only by oxygen isotope analysis (Eicken et al., 1994; Massom et al., 2001). Snow-ice is reported in the literature as ubiquitous in the southern hemisphere, albeit based on fairly limited in-situ observations (Massom et al., 2001). Jeffries et al. (1994) found snow-ice layers in floes at all but one of the sites they sampled in the West Antarctic in late summer 1992, and Lytle and Ackley (2001) suggested that continuous snow-ice production in the Weddell Sea is balanced by extensive ice basal melt, owing to the ocean heat flux in this region. For in-situ observations from two cruises conducted in winter 1994 and autumn 1995 in West Antarctica, Sturm et al. (1998) reported a remarkably consistent ratio of 1:1.2 snow depth to snow-ice thickness, equivalent to 55% of snowfall being converted to meteoric ice (Figure 6 of Sturm et al., 1998). Similarly, Jeffries et al. (2001) suggested that around half of the snow accumulation in the Pacific Ocean sector is entrained as snow-ice.

Given the difficulty in extrapolating sparse in-situ data to the wider scale, efforts have been undertaken to quantify snow-ice from remote sensing. Maksym and Markus (2008) estimated snow-ice thickness as the difference between PM (SSM/I) snow depths (Section 2.2.3) and snowfall from ERA-40 atmospheric reanalysis. Snow-ice was found in all regions of the Antarctic throughout the winter growth season (April–October), though in some places SSM/I snow depth exceeded snowfall, highlighting an error in one or both data sets. In contrast to previous studies, the authors found no dependence of snow-ice thickness on snow depth, and instead found snow-ice production to be driven by variability in snowfall. Surprisingly they also found no correlation between snowfall and snow depth and almost no seasonal variability in basin-average snow depth, casting doubt on the ability of PM observations to capture the seasonal evolution of the snow cover (Kern & Ozsoy-çiçek, 2016; Maksym & Markus, 2008).

Since our aim is to model the snow load from atmospheric reanalysis, we cannot follow the approach of Maksym and Markus (2008) to estimate snow-ice production. Further, due to the sparse spatial and temporal coverage of snow-ice surveys from ice cores, and uncertainty around the viability of extrapolating point measurement to the wider scale (Wever et al., 2021), we cannot accurately model snow-ice production as a function of region or season. Therefore, based on the results of Sturm et al. (1998), we choose a fixed percentage of 55% snow-ice production in our model, that is; 45% of the daily snow accumulation (after blown losses to the ocean) remains on the floe surface and 55% is lost (submerged, flooded and entrained as snow-ice). As well as being supported by literature, our choice is motivated by considering the range of what is physically possible. The amount of snow entrained as snow-ice could be anywhere in the range from zero (in the case of ice thick enough to support snow loading, as is generally the case in the Arctic), to 100% (e.g., where ocean heat flux keeps sea ice thickness constant, Maksym & Markus, 2008). Short of being able to model snow-ice production, which would require a-priori information on ice thickness, density, and ocean conditions, we choose a value near the middle of this range, which is supported by field data, and consider how the potential error of approximately ±50% affects our modeled snow depths (Section 3.2).

2.2. Validation Data

2.2.1. Ship-Based Snow Depths

The Antarctic Sea ice Processes and Climate (ASPeCt) data archive contains data compiled from more than 80 icebreaker voyages operating in the Antarctic sea ice zone between 1981 and 2016 (Kern, 2020; Worby, Geiger, et al., 2008), shown in Figures 2b and 2c. Snow depth and ice thickness were estimated on the level parts of floes, turned sideways as ships cut through the ice. The measurements are therefore not representative of the variable snow conditions that occur over deformed and very thick ice and should be taken as a lower bound (Worby, Geiger, et al., 2008). Since snow depths were estimated from the deck of the moving ship and not in-situ, they are unlikely to be accurate to the cm scale; Worby, Geiger, et al. (2008) assign an error of 20% for snow depth >30 cm. However, we assume that the spatial variability of snow depth along ship-transects is well captured by this method. The flooding and refreezing of basal snow would presumably complicate the ability to differentiate snow from sea ice in upturned floes. However, analyses from sea ice cores comment on the inability to distinguish sea ice from snow-ice without oxygen isotope analysis, therefore we trust that snow-ice is included in the ASPeCt "ice" measurement and that "snow depth" refers only to un-flooded snow above the water line. Despite its shortcomings, the ASPeCt archive is the only spatially and temporally extensive data set of in-situ snow depth that exists at present.

The data are publicly available via the University of Hamburg website (https://www.cen.uni-hamburg.de/en/icdc/data/cryosphere/seaiceparameter-shipobs.html). For the purposes of our study, ASPeCt data are averaged along 50 km segments of ship track. The mean snow depth is positioned at the mean of the input locations. The date stamp for the sample is the mean date of the input points. In areas of thick ice where ships move slowly, there can be multiple ASPeCt records at the same location. This clustering of measurements can bias the segment-average snow depth (Worby, Geiger, et al., 2008), therefore we omit any measurement within 1 km of the previous one. To form ASPeCt-CASSIS pairs for model calibration (Section 2.3), all CASSIS Lagrangian points on the day of the ASPeCt track and within 50 km of the ASPeCt segment-average location are averaged, producing CASSIS snow depth and ice age at the ASPeCt location. For comparison of model and PM climatologies (seasonal averages) to the ASPeCt climatology (Section 3.3), all ASPeCt 50 km-segment-means are averaged by season on a 2° latitude by 5° longitude grid.

2.2.2. Airborne Snow Depths

NASA operated its airborne Operation IceBridge (OIB) campaign over sea ice in the Antarctic between the years of 2009 and 2018. Although the aircraft carried a Snow Radar, snow depths estimated using this instrument have not been made publicly available as is the case for the Arctic. Kwok and Maksym (2014) developed an algorithm to derive snow depth from IceBridge snow radar data acquired during eight flights in October of 2010 and 2011. The snow depth estimates are available on request, but the data set is biased towards thick snow depths where the air/snow and snow/ice interfaces were easily distinguished in the radar echograms (Kwok & Maksym, 2014). To correct for this, the authors use the distribution of freeboards along segments of track to correct the distribution of snow depths. We use these bias-corrected segment-average snow depths, provided in Tables 2 and 4 of Kwok and Maksym (2014), combined with ground-track coordinates from the L2 OIB product available through NSIDC, to validate our model (Section 3.3.2).

2.2.3. Passive Microwave Snow Depths

Snow depths estimated from PM signatures are available from NASA GSFC for the period 1992–2007 (from the SSM/I sensor), and from the NSIDC for the period 2002–2011 (from the AMSR-E sensor aboard the AQUA satellite (Cavalieri et al., 2014)) and 2012-present (from the AMSR2 sensor aboard GCOM-W1 mission (Meier et al., 2018)). Hereafter we refer to the NASA GSFC SSM/I data set as "SSM/I," and the combined AMSR-E, AMSR2 data set as "AMSR." SSM/I snow depths are provided daily, whilst AMSR snow depths come as 5-day running averages to minimize the impact of data dropouts caused by thaw-freeze events. SSM/I(AMSR) data are projected on the NSIDC 25 km (12.5 km) Polar Stereographic grid. As well as being sensitive to meteorological and snow conditions, PM snow depths have an upper bound of 50 cm owing to the limited microwave penetration depths at 19 and 37 GHz frequencies.

2.3. Model Description

We split the Antarctic region into six sectors for the purposes of model initialization following the definitions of Worby, Geiger, et al. (2008) (Figure 2b). The western and eastern Weddell Sea are divided into two sectors, as the former is ice-covered year-round and contains as much as 80% of Antarctica's multi-year ice while the latter is essentially ice-free in summer (Worby, Geiger, et al., 2008). The model domain is a 10 km polar stereographic projection with a tangential plane of 70°S, and Lagrangian points are initialized on 20 February—the approximate date of the sea ice minimum extent—every year (1981–2021). On this date, SIC is linearly interpolated at the location of each Lagrangian point, and all points with a SIC greater than or equal to 15% are classed as "live." It is common for Southern Ocean sea ice to have a substantial snow layer at the time of its minimum extent (Webster et al., 2018). To estimate the depth of the initial snow layer, we utilize snow depths from the ASPeCt data archive (Section 2.2.1). All live points are initialized with a sector-dependent snow depth, calculated as the average of all ASPeCt snow depths recorded between January and March 1981–2016 within each sector (Figure 2b).

Following initialization, Lagrangian points are moved daily using sea ice motion vectors derived from satellite data (Section 2.1.2). Motion vectors are provided on a 25 km grid, which is linearly interpolated at the location of each Lagrangian point. Antarctic sea ice motion leads predominantly to divergence of Lagrangian points, especially in the Ross Sea coastal polynya where an estimated 180 cubic kilometers of sea ice is produced each winter (Dai et al., 2020). Where Lagrangian points diverge, new "live" points are created and are initialized with zero snow depth to simulate the refreezing of leads. To determine if divergence is sufficient to create a new Lagrangian point, the locations of the initial 10 km grid are examined. A new Lagrangian point is created if no others can be found within 25 km of the location on the initial grid and the SIC equals or exceeds 15%. In testing we found that the 25 km threshold was a good compromise, allowing the model to detect regions of large and continuous divergence while preventing excessive infilling over the whole ice extent and hence biasing the final gridded snow depth low. Such biasing could be overcome by accurately representing sea ice convergence, but this is currently excluded from the model. Instead we omit regions of small-scale ice divergence with an assumption that this is compensated elsewhere by small-scale convergence. New Lagrangian points are created daily as the sea ice extent expands: Ice-covered points (where SIC $\geqq$ 15%) are again moved using the motion vectors and ice-free points (SIC $<$ 15%) have their snow depth reduced to zero.

At each time step, ice-covered points accumulate snow from the atmosphere (derived from ERA5 atmospheric reanalysis (Hersbach et al., 2023)), and blown off the ice sheet (derived from the RAMCO2 regional climate model) (Sections 2.1.3 and 2.1.4). Snow is only accumulated at ice-covered points where the ERA5 daily maximum 2 m air temperature is below 0°C (Section 2.1.3). As with the previous inputs, snowfall grids are linearly interpolated at the location of each Lagrangian point. As described in Section 2.1.5, we employ the relationship derived in Sturm et al. (1998), and allow 55% of snowfall (after loss of snow blown into the ocean has been accounted for) to be entrained as snow-ice, leaving 45% to accumulate on the sea ice surface. We assess the sensitivity of our modeled snow depths to this treatment of snow-ice formation in Section 3.2. To calculate daily snow depth, we convert the column of accumulated SWE using daily snow densities estimated from in situ observations (Figure 2a). We convert the whole column of SWE to snow depth for each time step because the daily snow density function represents the mean of the whole column, not just the daily amount added (Massom et al., 2001). This is then added to the initial (20 February) snow layer.

Accumulated snow can be lost to the ocean if it is blown off sea ice floes. To estimate this we follow the method of Petty et al. (2018) for the Arctic, adapted for Antarctica using the 7 m s^{-1} minimum wind speed threshold for snow transport (U_t) identified by Andreas (1995). The amount of snow lost to the ocean every second (h_s^{bs}) is proportional to windspeed (U), open water fraction (f_{OW} = 1—sea ice concentration/100), and the depth of the accumulated snow layer (h_s), as follows:

$$h_s^{\mathrm{bs}} = \beta h_s U f_{\mathrm{OW}} \text{ for } U > U_t. \quad (1)$$

The proportionality constant β is allowed to vary freely in the model until a best fit to the in-situ observations is achieved. We assess this by comparing ship-based snow depths to coincident model snow depths, that is, ASPeCt-CASSIS pairs (Section 2.2.1). Both are plotted as a function of ice age, where ice age is the number of days that a Lagrangian point has been "live" (Figure 3a). To reduce noise, data are averaged in 10-day age bins, however after 270 days averages become increasingly noisy as fewer and fewer ice parcels reach these ages. We therefore exclude data older than 270 days from the comparison. β is adjusted until the mean difference and

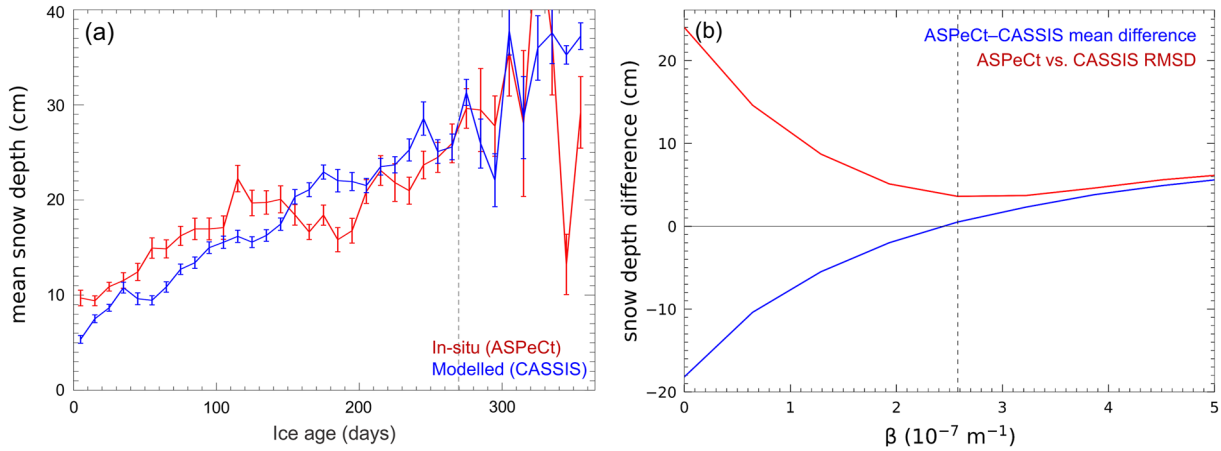

Figure 3. Calibration of β, the blowing snow parameter. (a) ASPeCt-CASSIS pairs (Section 2.21) plotted as a function of ice age. Ice age is defined as the number of days that a point has been "live." Error bars show the 1-sigma standard deviation on the 10-day (binned) mean. Note that after age 270 days, shown by the dashed gray line, data become increasingly noisy as fewer ice parcels survive, and we therefore exclude data beyond day 270 when comparing the timeseries mean and root-mean-square deviation (RMSD). The plot shows model snow depths for $\beta = 2.6 \times 10^{-7}$ m^{-1}, which was selected by allowing β to vary freely until a best fit to the in-situ data was achieved. (b) The best fit is defined as the smallest absolute mean difference and RMSD between model and in-situ snow depths as a function of ice age (for age <270 days). The dashed gray line shows the position of the returned value, $\beta = 2.6 \times 10^{-7}$ m^{-1}.

root-mean-square deviation (RMSD) between model and in-situ snow depths are at a minimum (Figure 3b), achieved at $\beta = 2.6 \times 10^{-7}$ m^{-1}. The reason that we use ice age to calibrate β is because:

Without the loss term, snow would continually accumulate on pixels as long as they were live. The purpose of the loss term is to moderate this build-up to something realistic, which we assess therefore against the accumulation of snow in the in-situ data (Note that ice age comes from the model and is therefore common across both data sets; there is no record of ice age within the in-situ data set itself).

Our loss term is very crude; it does not account for the shape of the opening (lead, polynya) and snow is not blown in the direction of the wind. Further, since it is tuned to fit the observations, it could reasonably be considered as a more general loss term which integrates other processes, for example, atmospheric sublimation and snow melt, which we do not account for separately. This is discussed in Section 4.3.

Our model tracks Lagrangian points and their associated snow depths at daily resolution. At the end of each day, we average the snow depths of all live Lagrangian points within a 50 km radius of each original 10 km grid point center to produce a smoothed gridded output. Since the model does not account for small-scale localized processes such as ridging, wind redistribution of snow (into e.g., sastrugi), snow metamorphism, rain-on-snow and melt events, the smoothing does not eradicate small-scale snow depth variability which we would otherwise wish to preserve. The 50 km radius was chosen in order to ensure that enough Lagrangian points are included in the smoothing to reduce the noise (points can be separated by more than 25 km at the end of each timestep).

2.4. Validation and Trend Analysis

For comparison of CASSIS to ASPeCt and PM snow depths, we average daily 10-km gridded snow depth maps from the model per year and season. We then average the years to form a seasonal climatology. The range of years that form the climatology depend on the data set we are comparing to. For model validation with in-situ ship data (Section 3.3.1), the gridded values in the APSeCt map for each season (Section 2.2.1) are paired with the nearest ones from the 1981–2016 model climatology. We form seasonal climatologies of the PM snow depths in the same way as the model data. These are then regridded to 10 km for comparison to the CASSIS climatology, which we generate over the same time period as the PM data set (1992–2007 for comparison to SSM/I and 2003–2020 for comparison to AMSR). For comparison to the airborne data (Section 3.3.2), the CASSIS map for each day of the OIB flight is sampled along the flight path.

To estimate the seasonal trends (Section 3.4), daily 10-km snow depth grids from 1981 to 2021 are averaged per year and per season. This forms, for each season, a 41-year time series at each 10 km grid cell location. We apply linear regression to each grid cell time series to form a trend map for each season. Any grid cell which has a value

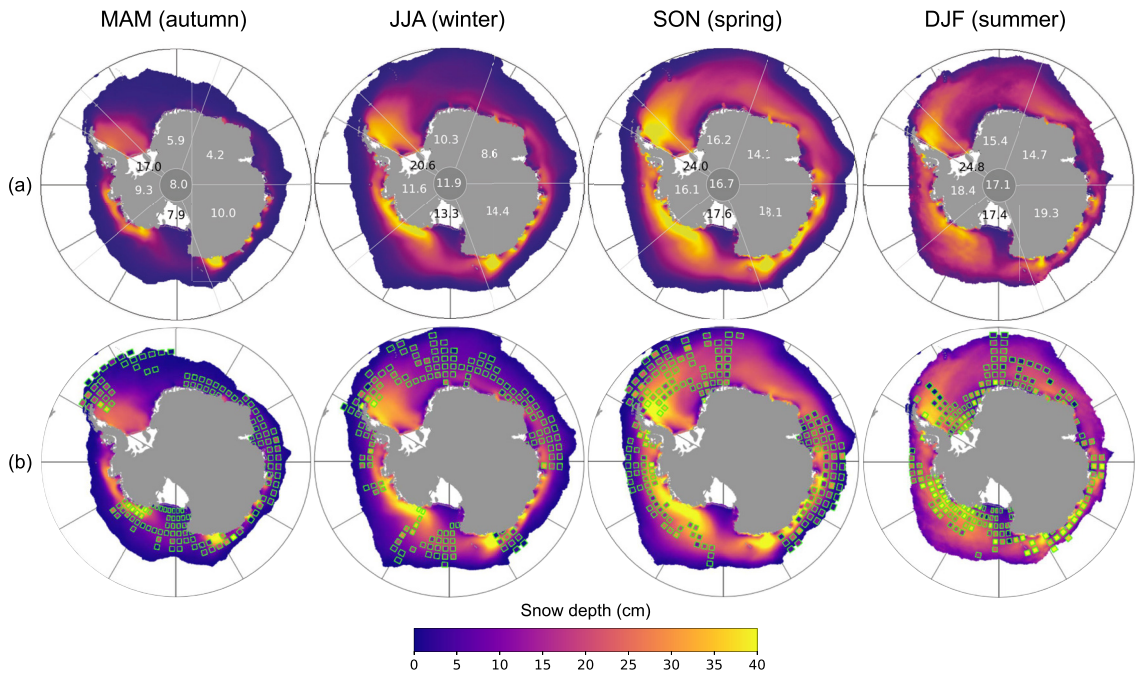

Figure 4. (a) Seasonal-average CASSIS snow depth over the ASPeCt period (1981–2016). Average values for each sector (defined in Figure 2) are shown. The central value is the circumpolar average. (b) CASSIS snow depth over the ASPeCt period (1981–2016) overlain with ASPeCt ship data for 1981–2016 averaged per season in 2° latitude by 5° longitude cells. Sector-average snow depths for CASSIS and ASPeCt are detailed in Figure S1 in Supporting Information S1.

of zero snow depth for all 41 years is excluded from the trend calculation, since these represent areas which have been snow free for the entire period.

3. Results

3.1. Snow Depth Climatology

Figure 4 and Figure S1 in Supporting Information S1 show the simulated snow depth climatology, derived by averaging daily model output for 1981–2016 by season and year, and the averaging the years together. Despite evident seasonal evolution (growth) of the snowpack, the spatial distribution of snow remains similar all year, with a general pattern of deeper snow near the coast becoming thinner towards the ice edge. This pattern results from the manner in which sea ice grows in the southern hemisphere—northwards from the ice sheet margin (Maksym, 2019), which allows floes formed nearer the continent more time to accumulate snow. A notable exception to this pattern is the southern Ross Sea, where thin snow persists year-round due to the constant formation and redistribution of ice at coastal Polynyas (e.g., Bromwich & Kurtz, 1984). Thin snow (<10 cm) also persists throughout the year along the coast of the Weddell East sector and much of the Indian sector, attributed to offshore winds and polynya formation (Kern, 2009; Tamura et al., 2008). The thickest snow is found in the west Weddell Sea, and the coastal Amundsen and Indian South East sectors, reaching depths of +40 cm by the end of the growth season (Figure 4a). The spatial distribution and magnitudes of snow depths agree to first order with recently emerging products from dual-altimetry (Garnier et al., 2021; Kacimi & Kwok, 2020). In particular, finer spatial details such as the occurrence of thin snow along the coast of the East Weddell sector, are also evident in the snow depth product from differencing laser and radar freeboard retrievals (Kacimi & Kwok, 2020, Figure 3 [September–October]).

3.2. Snow-Ice Sensitivity

The absence of error estimates for ERA5 reanalysis data precludes a formal uncertainty assessment of our snow depth product. However, given that snow-ice formation is a highly variable and complex process, our simplistic assumption that 55% of daily accumulation is entrained as snow-ice arguably represents one of the largest uncertainties in our model. Therefore, in this section, we analyze the sensitivity of our modeled snow depth estimates to snow-ice formation, and use this to estimate snow depth uncertainty.

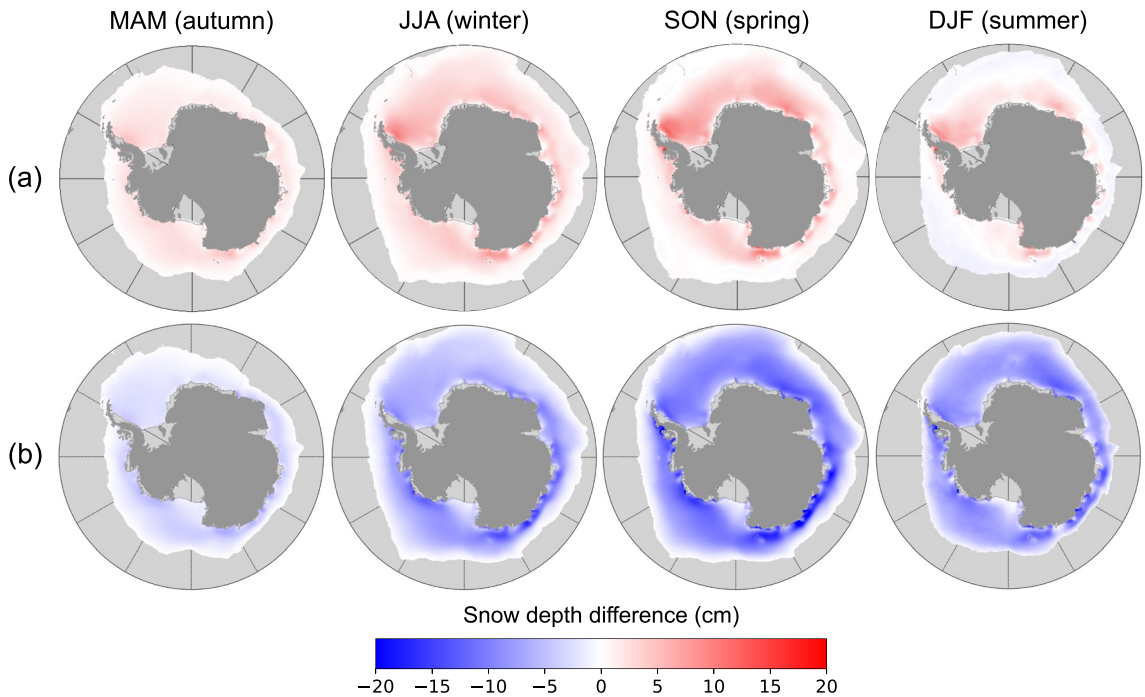

Figure 5. Exploring model sensitivity to snow-ice formation. (a) Climatology of $CASSIS_0$–CASSIS differences where CASSIS is our nominal model output, run with $\beta = 2.6 \times 10^{-7}$ m^{-1} and $\alpha = 0.55$ (Equation 1), and $CASSIS_0$ is the 0% snow-ice formation run where $\beta = 2.6 \times 10^{-7}$ m^{-1} and $\alpha = 0$. (b) Climatology of $CASSIS_{100}$–CASSIS. $CASSIS_{100}$ is the 100% snow-ice formation run, where $\beta = 2.6 \times 10^{-7}$ m^{-1} and $\alpha = 1$.

We explore our model's sensitivity to snow-ice by implementing two extreme cases whilst keeping β fixed at its calibrated value (2.6×10^{-7} m^{-1}):

(i) 0% snow-ice formation. All of the daily-accumulated snow remains on the floe surface. The difference between this run ($CASSIS_0$) and our standard model climatology (CASSIS) is shown in Figure 5a.

(ii) 100% snow-ice formation. No snowfall remains on the floe surface and therefore the only snow cover is the initialized layer. This case ($CASSIS_{100}$) minus our model climatology (CASSIS) is shown in Figure 5b.

The spatial pattern of $CASSIS_0$–CASSIS differences is predominantly positive, reaching maximum values of ∼20 cm in the winter and spring in the West Weddell sector and the easternmost part of the Indian South East sector, near the coast. In summer, differences generally decrease everywhere, becoming slightly negative (∼2 cm) at the outer edges of the ice pack, highlighting the dominant role of loss of snow blown into the ocean in the summer. To understand this distribution of differences we recall that to simulate the formation of snow-ice, we remove a proportion of the daily accumulated snow *after* blowing snow processes have been accounted for (Section 2.4). That is, the total amount of snow, H_s, is given by:

$$H_s = h_s + (1 - \alpha)\left(\mathrm{sf} - h_s^{\mathrm{bs}}\right),$$

where α is the snow-ice fraction, h_s is depth of the existing snow layer, sf is snowfall (from atmosphere and ice sheet) and h_s^{bs} is the snow blown into the ocean, given by Equation 1. For our nominal model run CASSIS therefore:

$$H_s = h_s + 0.45(\mathrm{sf} - \beta h_s U f_{\mathrm{OW}}), \tag{2}$$

whilst for case $CASSIS_0$:

$$H_{s\_a} = h_{s\_a} + (\mathrm{sf} - \beta h_{s\_a} U f_{\mathrm{OW}}). \tag{3}$$

Since β is kept fixed, only the depth of the existing snow column causes the amount of snow blown into the ocean to differ between CASSIS and $CASSIS_0$. However in CASSIS, both the snowfall and the blown snow are then reduced by ∼half due to snow-ice formation. Following initialization (both runs are initialized with the same ASPeCt-average snow depths, Section 2.3) H_{s_a} will always exceed H_s if snowfall outweighs blown snow lost

to the ocean, that is, if the term inside the brackets is positive (tested for realistic values of sf, U, f_{OW}). This is the case in autumn, where $CASSIS_0$–CASSIS differences are everywhere positive. The largest differences occur in the West Weddell and the eastern coast Indian South East sectors, where the open water fraction (f_{OW}) and windspeed (U) are low (Figure S2 in Supporting Information S1). Since little snow is lost to the ocean in these regions, snowfall accumulates on top of the initialized snow cover more rapidly in $CASSIS_0$ than CASSIS. The same pattern continues into winter, with positive differences increasing in the thick-snow regions of the Weddell Sea and coastal Indian South West and East sectors. Along this coastline, small pockets of zero difference emerge where wind speeds are high. In these regions, the snow blown dominates over snowfall, preventing H_{s_a} from becoming bigger than H_s. In the spring, the $CASSIS_0$–CASSIS difference in the fringes of the sea ice cover has reduced. This can only happen if more snow is blown into the ocean than falls on the ice, therefore this marks the perimeter where the wind becomes sufficiently strong and open water fraction sufficiently high for blown snow to exceed snowfall and the term in the brackets become negative. Note that because h_{s_a} initially exceeds h_s, the term in the brackets of Equation 3 will become negative (with sufficient wind and open water fraction) before Equation 2, that is, snow depths in $CASSIS_0$ will begin to decrease due to snow blown into the ocean whilst still increasing in CASSIS, thereby reducing the positive difference between the two. In summer, low snowfall, high winds and the break-up of the ice pack resulting in high open water fraction (Figure S2 in Supporting Information S1) combine to cause a net removal of snow in both CASSIS and $CASSIS_0$. Differences reduce everywhere as H_{s_a} is more readily eaten away at by the wind than H_s, becoming slightly negative at the sea ice edge where the spring difference was near-zero.

Since in $CASSIS_{100}$ all snowfall is converted to snow-ice and none accumulates on the surface, the only snow cover throughout the year is the initialized layer. The climatology of $CASSIS_{100}$–CASSIS differences (Figure 5b) therefore highlights regions of snow accumulation, which is most abundant in the coastal Bellingshausen & Amundsen and Indian South East sectors where open water fraction is low and snowfall relatively high all year (Figure S2 in Supporting Information S1). Differences increase between autumn and spring as the snow layer in CASSIS accumulates, and then falls off slightly in summer as CASSIS loses blown snow to the ocean.

Since we consider our treatment of snow-ice to be the largest source of uncertainty in our model, and since the seasonal spatial differences capture the sensitivity of the model to snow-ice formation, we treat Figures 5a and 5b as a first-order estimate of the upper and lower bounds of the uncertainty on our modeled snow depths. There are many other model parameters which will influence our snow depth estimates, including the initialization snow depth, the choice of reanalysis, SIC and sea ice motion data sets, and our snow density function. A comprehensive sensitivity analysis exploring the effect of these on our model is beyond the scope of this study.

3.3. Model Validation

3.3.1. Comparison to In-Situ Ship Data

We analyzed the seasonal differences between model and ship-based estimates of snow depth from ASPeCt to assess model performance. Since the ASPeCt snow depths were used in the calibration of the model (Section 2.3), this cannot be considered as an independent validation. However, because the calibration utilized data as a function of ice age, the regional and seasonal performance of the model can still be assessed using the ASPeCt data. Taking each ASPeCt grid cell in Figure 4b as a single observation, CASSIS snow depths are on average 1.9 cm thinner than ASPeCt with an RMS difference of 13.1 cm (Figure 6a). Model snow depths are 1.8 cm thinner than the ship-based observations in autumn (March to May), where ASPeCt exceed CASSIS in all regions except the Ross Sea (Figure S1 in Supporting Information S1); comparable in winter (June to August); and 0.8 cm thicker in spring (September to November) most notably in the Ross and Indian South West sectors (Figure S1 in Supporting Information S1). Differences are greatest in summer (December to February), at the end of the model run, when CASSIS estimates are thinner in all sectors except the western Weddell, and by 6.3 cm on average. The model is initialized towards the end of February, and so we might expect the agreement with in-situ observations to be strongest in autumn and to deteriorate thereafter as uncertainties accumulate over time. It is, however, difficult to separate the model's performance through the year from seasonal differences in sampling. For example, referring to Figure 4b, we find that the southern Weddell Sea is sampled by ships only in the summer. We cannot therefore rule out the possibility that snow depth is underestimated in this area all year, rather than solely during the summer when we observe large differences between CASSIS and ASPeCt. It may be that our model under-performs in this region all year due to snowpack processes unique to the area. We assess CASSIS against ASPeCt in more detail in Sections 3.3.3 and 4.1.

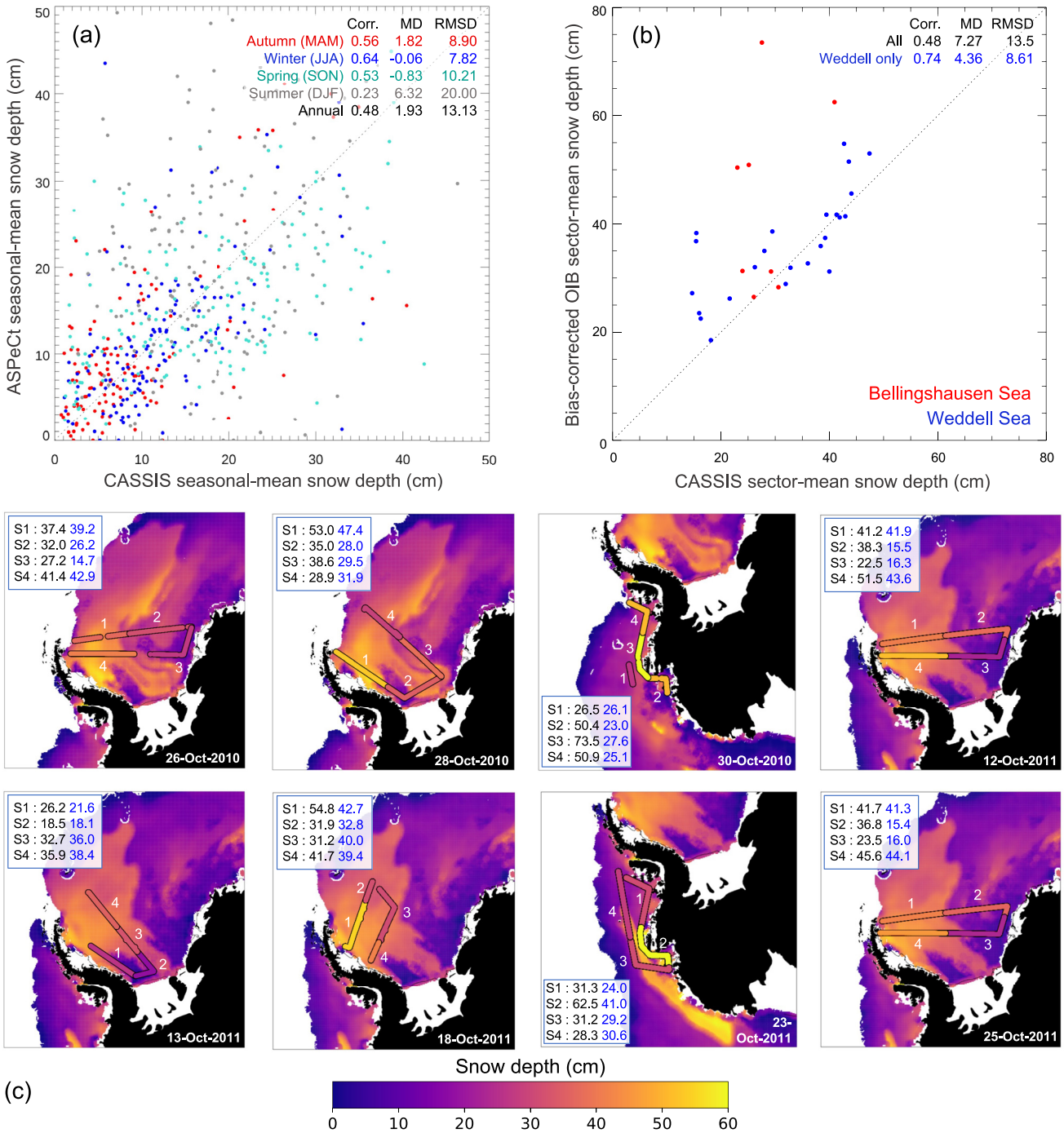

Figure 6. Model validation. (a) Scatter plot of in-situ (ASPeCt) versus model (CASSIS) snow depths, colored by season. Correlation = 0.48, mean difference (ASPeCt−CASSIS) = 1.9 cm, root-mean-square deviation (RMSD) = 13.1 cm. (b) Model (CASSIS) versus airborne (Operation IceBridge [OIB]) snow depths from the Weddell (blue) and Bellingshausen (red) seas. Correlation, mean (OIB–CASSIS) difference and RMSD for all (Weddell only) points are 0.48(0.74), 7.27(4.36) cm and 13.5(8.61) cm. (c) Airborne (OIB) snow depth segments (from Kwok & Maksym, 2014) overlain on model (CASSIS) snow depth for the same day. Segment-average snow depths (cm) for OIB (black) and CASSIS (blue) are shown in the boxes.

3.3.2. Comparison to Airborne Data

As a second evaluation, we compared our modeled snow depths to estimates derived from eight Operation IceBridge flights in the Weddell and Bellingshausen Seas in October 2010 and 2011 (Kwok & Maksym, 2014) (Section 2.2.2). The modeled depths are on average 7.3 cm thinner than the airborne estimates and the root mean

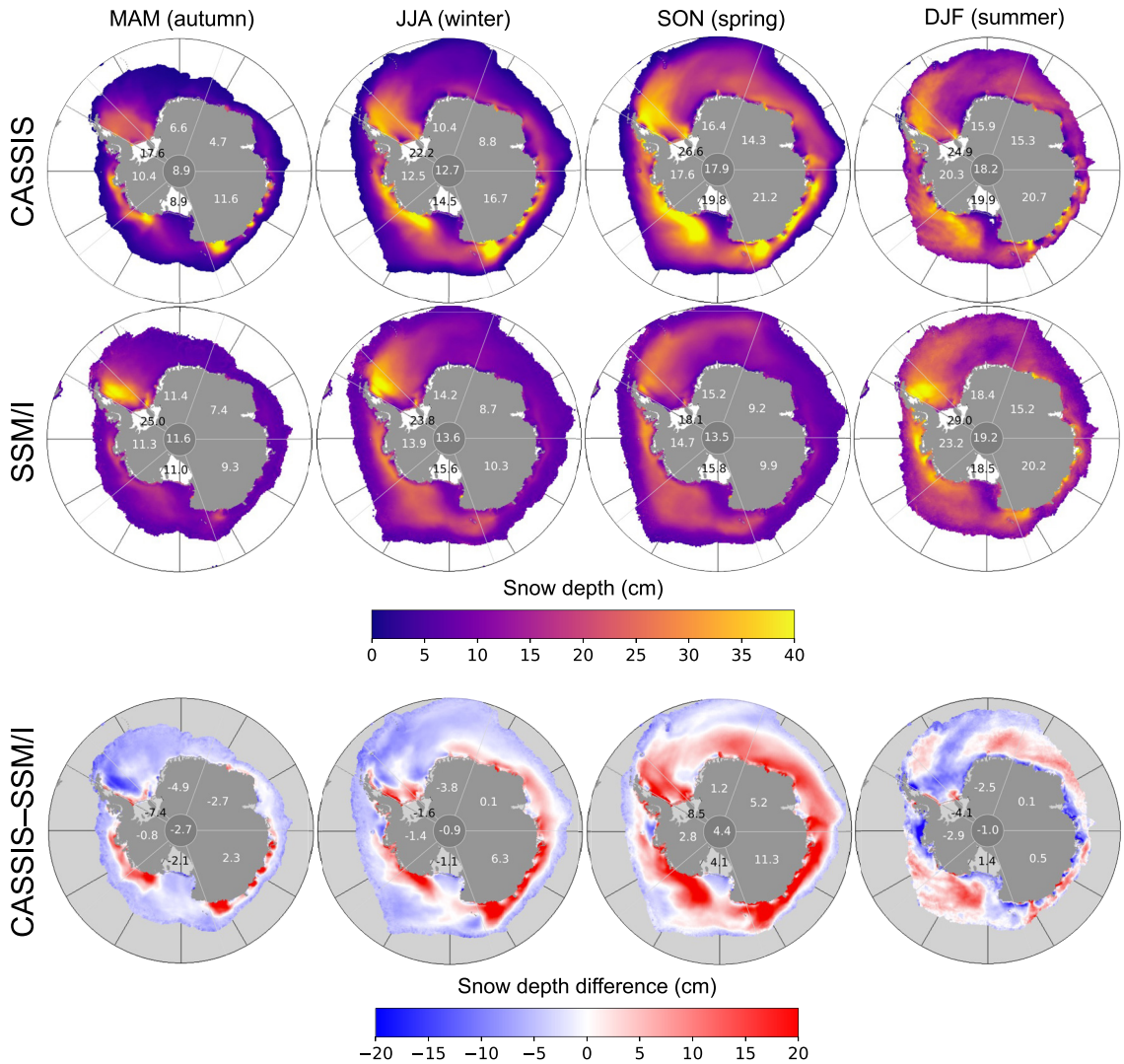

Figure 7. CASSIS versus Special Sensor Microwave/Imager (SSM/I) over the common period from 1992 to 2007. Average values for each sector (defined in Figure 2) are shown. The central value represents the circumpolar average. CASSIS and SSM/I climatologies compared to ASPeCt data over the same period (1992–2007) are shown in Figure S3 in Supporting Information S1.

square difference is 13.5 cm, with the closest agreement in the Weddell Sea (r = 0.74, Figure 6b), suggesting that our model performs better in this sector than in the Bellingshausen Sea. Airborne snow depths recorded in the Bellingshausen Sea exceed 60 cm in places, and although on 23 October 2011 modeled depths are high (40–50 cm) in this region, they do not reach this level and are not coincident in space. On 30 October 2010, modeled snow depths do not exceed 40 cm. Analysis of the airborne data reveal a strong correlation between snow depth and surface roughness, suggesting higher accumulation over deformed ice which can trap falling and wind-blown snow (Kwok & Maksym, 2014). The discrepancy between model and airborne estimates in the Bellingshausen Sea may therefore be highlighting a wider issue; snow depth is likely underestimated in rough ice areas because increased snow accumulation over deformed ice is not accounted for in the model. We discuss this further in Section 4.3.

3.3.3. Comparison to Passive Microwave Snow Depths

Figure 7 (Figure 8) shows the difference in seasonally-averaged snow depths from CASSIS and SSM/I(AMSR) for their period of overlap from 1992 to 2007 (2003–2020). Despite notable differences in the prevalence of thick snow (>35 cm), the general pattern of snow depths from CASSIS and PM is similar. This is reassuring given the

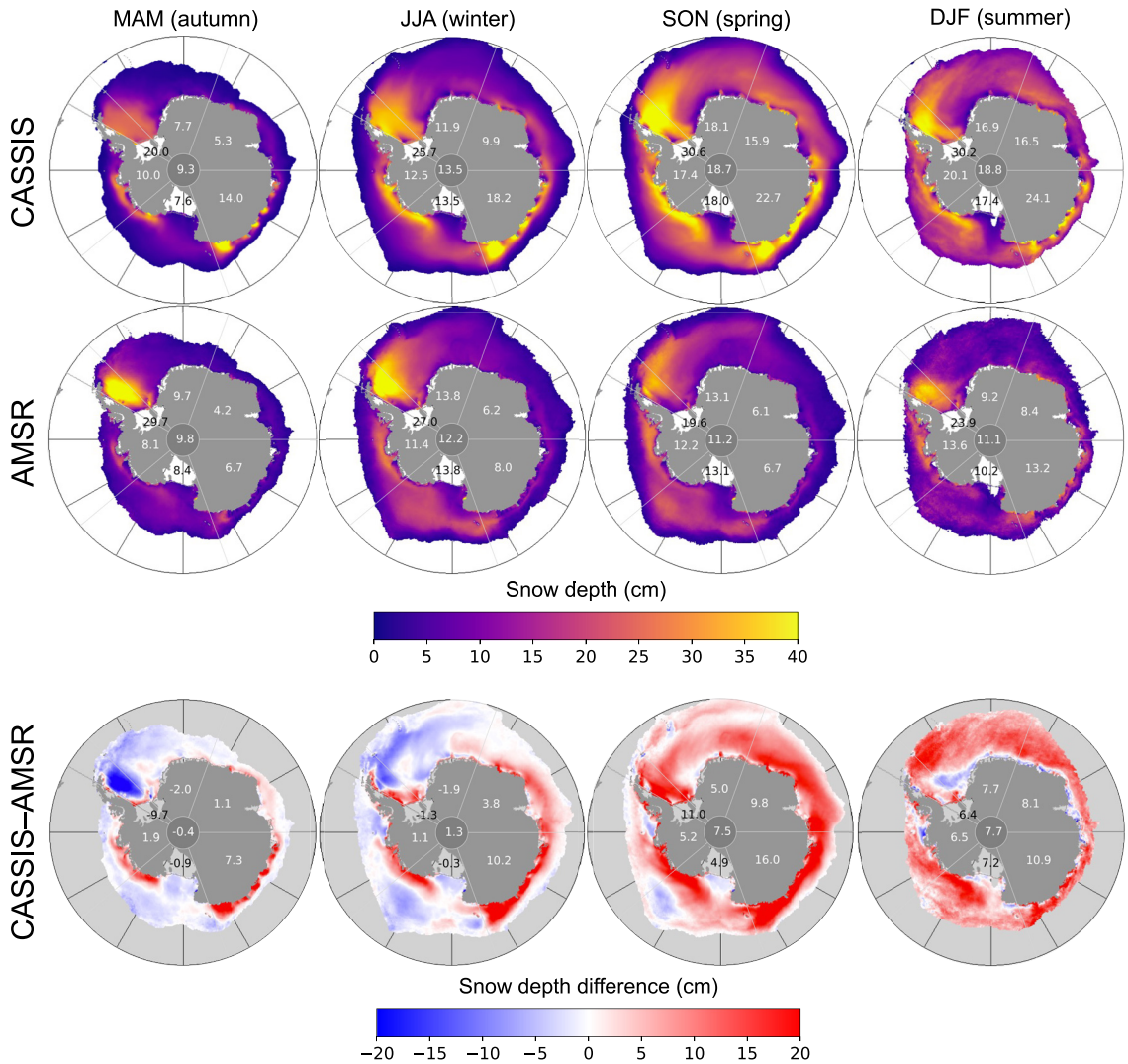

Figure 8. CASSIS versus Advanced Microwave Scanning Radiometer (AMSR) over the common period 2003–2020. Average values for each sector (defined in Figure 2) are shown. The central value represents the circumpolar average. CASSIS and AMSR climatologies compared to ASPeCt data over the common period (2003–2016) are shown in Figure S4 in Supporting Information S1.

entirely different retrieval approaches (model-driven vs. satellite-observed) and suggests some truth in both data sets.

The pattern of CASSIS–SSM/I and CASSIS–AMSR differences are broadly the same in autumn; modeled snow depths exceed PM over the older ice that fringes the continent and are smaller than PM snow depths over the younger ice further north, most notably in the West Weddell sector where the largest CASSIS–SSM/I and CASSIS–AMSR differences occur (−7.4 and −9.4 cm). This general pattern of opposing negative and positive differences persists into winter, though the fringe where CASSIS exceeds PM has expanded and seemingly been transported northwards; a possible indication of areas of multi-year ice initialized with too-thick a snow cover. In spring, modeled snow depths are thicker than PM in all sectors, in particular for AMSR where differences are almost exclusively positive and modeled snow depths are on average 7.5 cm thicker. This shift towards predominantly positive differences results from a notable difference in the growth of the modeled and PM snowpacks; while CASSIS snow depths increase significantly (by ∼5 cm) between winter and spring, PM snow depths decrease slightly (−1 mm for SSM/I and −1 cm for AMSR).

Interestingly, the pattern of CASSIS–SSM/I and CASSIS–AMSR differences are dissimilar in the summer. In the CASSIS data, areas of thick spring snow decrease by summer, though the circumpolar average remains high due

to the melting of the northernmost ice with thin snow cover. In the SSM/I data, snow depths increase from spring to summer over most of the sea ice pack and most notably in the coastal Bellingshausen & Amundsen, Indian South East and Weddell Sea sectors, bringing snow depth more in line with those from CASSIS. By contrast, AMSR snow depths remain relatively stable between spring and summer, continuing the pattern of positive CASSIS–AMSR differences in all sectors.

This difference between the PM data sets suggests that where snow depths used to increase between spring and summer (i.e., between 1992 and 2007), they no longer do (between 2003 and 2020). If such a trend resulted from variability in snowfall, we would expect our model to capture it, however an increase in snow-ice prevalence or surface melt, leading to smaller snow depths, would be uncaptured in our model.

In order to assess the performance of our modeled snow depths against those from PM, we turn again to the in-situ ship data. ASPeCt data for each season of the SSM/I and AMSR periods were averaged in 2° latitude by 5° longitude grid cells and compared to the coincident CASSIS and PM snow depths. Results are shown in Figures S3 and S4 in Supporting Information S1 and Figure 9. We compare seasonal averages (rather than daily measurements) in order to evaluate CASSIS, PM, and the difference between them in the context of conditions (meteorological, sea ice, ocean) associated with each season. Comparisons of SSM/I and AMSR snow depths to in-situ have been conducted before (Kern et al., 2011; Kern & Ozsoy-çiçek, 2016; Markus & Cavalieri, 1998; Worby, Markus, et al., 2008), though never over as long a period as we do here.

On average, SSM/I outperforms CASSIS in the autumn, yielding a better correlation and smaller mean difference and RMSD compared to the ASPeCt data (Figures 9a and 9b). However, the ASPeCt data are not uniformly distributed, and the circumpolar statistics are composed of regionally opposing signals. Unfortunately, there are no ASPeCt data In the Bellingshausen & Amundsen sector where we find large positive CASSIS-SSM/I differences, though in the Indian South East sector where CASSIS also exceeds SSM/I, CASSIS aligns more closely with the ASPeCt data (Figure S3 in Supporting Information S1). Thick snow depths in the West Weddell sector are well captured by SSM/I, but absent in the CASSIS data. In the winter, very little of the region where CASSIS snow is thick is sampled by ASPeCt, however the small amount of data in the east Indian South East sector suggests that snow is overestimated by CASSIS in this area, whilst underestimated by SSM/I. CASSIS agrees more closely with the in-situ data in the Ross, West Weddell and East Weddell, but underperforms compared to SSM/I in the Bellingshausen & Amundsen and Indian South West sectors. Overall SSM/I agrees better with the in-situ in winter (smaller RMSD and better correlation, Figures 9a and 9b). The same is true for the spring, where CASSIS exceeds SSM/I over most of the ice pack and over nearly all of the area sampled by the ASPeCt data. Again, performance relative to the in-situ data is regionally dependant, with CASSIS agreeing more closely with ASPeCt in the Bellingshausen & Amundsen and West Weddell and SSM/I performing better in the Weddell East, Indian South West, Indian South East, and Ross sectors. On average, CASSIS(SSM/I) snow depths are overestimated (underestimated) compared to the ASPeCt data. In summer, both CASSIS and SSM/I underestimate snow depth relative to the ASPeCt data in the Bellingshausen & Amundsen and Indian South East sectors, and overestimate it in the East and West Weddell sectors. Only in the Indian South West does the agreement vary, with CASSIS underestimating and SSM/I overestimating snow depth relative to ASPeCt. Given that CASSIS exceeds SSM/I over most of this sector (Figure 7), the comparison to ASPeCt is driven by the band of negative CASSIS-SSM/I differences near the coast.

Assessing the performance of CASSIS relative to AMSR is difficult due to a paucity of ASPeCt data over the AMSR period from 2003 to 2016. In autumn and winter, there is next to no in-situ data over the regions where CASSIS and ASMR snow depths deviate the most, though on average AMSR agrees marginally more closely with ASPeCt in the autumn, and less closely in the winter when CASSIS snow depths are within 1 mm of ASPeCt (Figures 9c and 9d). There are more ASPeCt data in the spring, though the Ross sector remains unsampled by ships. The growth of the CASSIS snow cover between winter and spring is supported by the ASPeCt data in the regions sampled—the Indian South West and Indian South East sectors, where AMSR underestimates snow depth by more than 10 cm, and in the West Weddell where AMSR snow depths (which have decreased since the winter) fall short of the ASPeCt snow depths. Conversely, in the East Weddell, where snow depths have also increased in CASSIS but decreased in AMSR, AMSR agree more closely with the in-situ data from ASPeCt. In the summer, the ASPeCt data exceed both CASSIS and AMSR in all regions sampled, namely the Ross, Bellingshausen & Amundsen and Weddell (East and West) sectors. Since the regions sampled by ASPeCt in the spring and summer are different, we cannot directly assess whether the

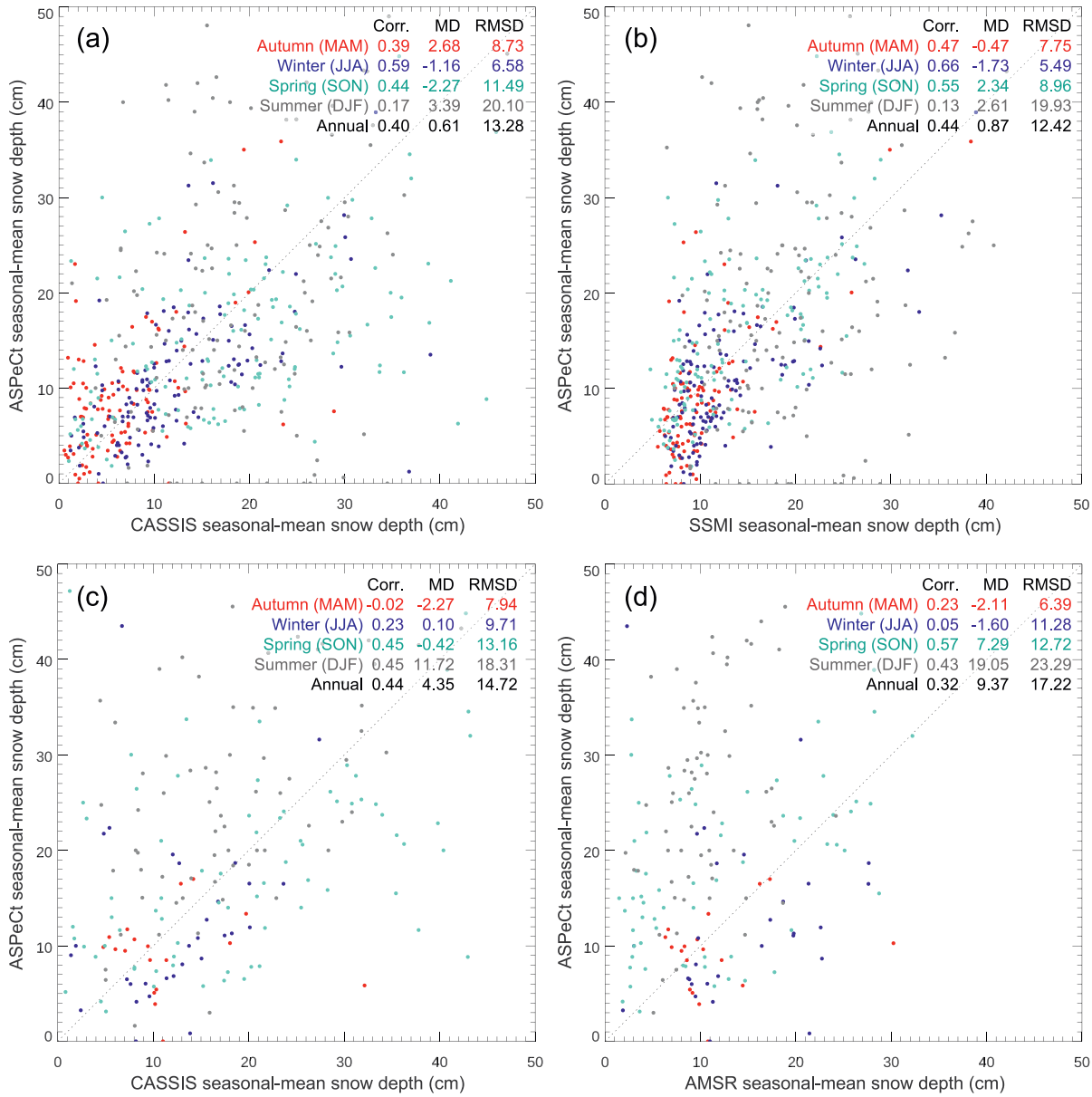

Figure 9. CASSIS, Special Sensor Microwave/Imager (SSM/I) and Advanced Microwave Scanning Radiometer (AMSR) versus ASPeCt. ASPeCt 50 km-segment-means are averaged by season on a 2° latitude by 5° longitude grid and plotted against the coincident model/passive microwave (PM) seasonal average. (a) CASSIS versus ASPeCt over the SSM/I period (1992–2007). (b) SSM/I versus ASPeCt over the SSM/I period (1992–2007). (c) CASSIS versus ASPeCt over the AMSR/ASPeCt period (2003–2016). (d) AMSR versus ASPeCt over the AMSR/ASPeCt period (2003–2016). Corresponding maps for (a) and (b) are shown in Figure S3 in Supporting Information S1 and for (c) and (d) in Figure S4 in Supporting Information S1.

snow cover increased between spring and summer, however the much smaller AMSR snow depths compared to ASPeCt in the regions sampled would suggest that a real seasonal growth signal is missing from the AMSR data.

Based on the root-mean-square differences (Figure 9), SSM/I agrees more closely with the ASPeCt data in all seasons, although snow depths <5 cm are overestimated (Figure 9b). AMSR performs worse than CASSIS overall, although the agreement to ASPeCt is slightly better in spring. Given that ASPeCt predominantly samples level ice where PM performs best (Comiso et al., 2003; Markus & Cavalieri, 1998), we suggest that comparisons to ASPeCt may be positively biased and not representative of the overall performance of snow depth estimates from PM.

3.4. Snow Depth Trends

Our model output allows us to chart temporal changes in the depth of snow on sea ice in the Southern Ocean between 1981 and 2021 (Figure 10). We compute trends by applying linear regression to modeled snow depths at each 10 km grid cell where all 41 years of simulations exist (Section 2.4). The overall pattern of snow depth trends is similar in each season (Figure 10a), with significant ($P \leq 0.05$) features being strong thinning of up to 6 mm/year in coastal sectors of the South Pacific Ocean (Bellingshausen, Amundsen, and Ross seas), and strong thickening of up to 6 mm/year in the Weddell Sea and in the Indian South East sector. Circumpolar annual-average snow depth increased by 16 mm between 1981 and 2021 ($P = 0.004$, Table S1 in Supporting Information S1). This is formed of competing signals; a negative trend of 13 mm in the South Pacific Ocean (P 0.133, but significant in autumn [$P = 0.012$] and summer [$P = 0.048$], Table S1 in Supporting Information S1), with an increase of 31 mm everywhere else ($P = 0.000$).

To explore the drivers of trends in snow depth, we recorded at daily intervals the contribution of the individual component terms to the total snow depth, and average by season (Figure 10). On any day, total snow depth comprises (b) the initialized snow layer (zero for all Lagrangian points created *after* 20 February) and (c) snow accumulated since initialization/creation, which is the sum of atmospheric snowfall, snow blown from the ice sheet by Katabatic winds (negligible), snow-ice formation, and snow blown to the ocean. We also separately computed the trend in ERA5 atmospheric snowfall (Figure 10d), which we scale by half since 55% of snowfall is immediately lost to snow-ice formation and does not therefore contribute to snow depth in the model. The trend in ice floe age (Figure 10e) is computed from daily tracking of Lagrangian points. Ice age trends do not solely reflect changes in the timing of ice formation and melt, but also trends in ice motion. For example, a tendency for ice to remain in a given area where it used to be transported elsewhere, will be shown as an increase in ice age in that area, despite the ice having formed at the same time. Conversely, an area which has experienced an increase in ice export will demonstrate a negative ice age trend. Determining the drivers of the ice age trends we observe would require a separate analysis of the SIC and drift data sets, which is beyond the scope of this study. The initial snow depth (b) is the dominant factor in the trend in snow depth in many regions—particularly the Bellingshausen & Amundsen sector, where it accounts for 89% of the signal in spring, decreasing to 63% in summer. Given that Lagrangian points within the 20 February sea ice extent mask are initialized with the same snow cover each year (the sector-average of all ASPeCt observations from January to March 1981–2016), trends in initial snow depth occur solely as a result of changes in the sea ice extent on this date (Figure 10f). The reason we apply a snow depth is to simulate the fact that ice remaining at the end of the melt season retains its snow cover going into the growth season. Since 20 February is around the sea ice minimum, we assume that all ice present on the 20 February is multi-year and initialize it with a snow depth. The more multi-year ice there is, the higher the autumn-average snow depth of the region. Therefore, trends in initial snow depth mirror trends in multi-year ice fraction and the decline in modeled snow depth in the South Pacific Ocean is the result of reduced summer ice extent in this region. The spatial pattern of trends in the initial term in each season results from the movement of initialized multi-year ice around the ocean, therefore areas which are dominated by seasonal ice all year show zero trend in the initialization component (Figure 10b). The remainder of the snow depth trend, that of the accumulated layer (Figure 10c), arises through the combined effects of snowfall from the atmosphere and continent, and snow lost to snow-ice formation and (blown into) the ocean. All of these contributions and subtractions tend to increase with ice age, because ice floes that exist for longer have more time to accumulate snow, a relationship also seen in the in-situ ASPeCt data (Figure 3a). This effect is larger than trends associated with snowfall, which are positive over most of the Southern Ocean (Figure 10d). Notably, spring and summer snow depth has declined the Indian South West sector and eastern Weddell sea, despite positive trends in snowfall, owing to decreased ice age in these regions. Conversely, reduced summer snowfall in the Indian South East sector has not led to reduced snow depth, due to the compensating effect of increased ice age in this region. In the southern Ross Sea, negative snow depth trends from autumn to spring result from reduced ice age (snowfall trends are negative but are not statistically significant in this region), and in summer an area of positive snow depth in the east emerges as a result of increased ice age and possibly snowfall, which is positive but not significant. This positive signal is also seen in the initial term, indicating an increased tendency for multi-year ice (with an initial snow layer) to exist in this area in the summer. In the northern Ross and Amundsen seas, positive snow depth trends from autumn to spring are attributed to increased snowfall and increased ice age.

It must be emphasized that this analysis of snow depth trends and their drivers is a model result. Since the ASPeCt data we use to initialize, calibrate and validate the model are temporally limited (e.g., no data in the

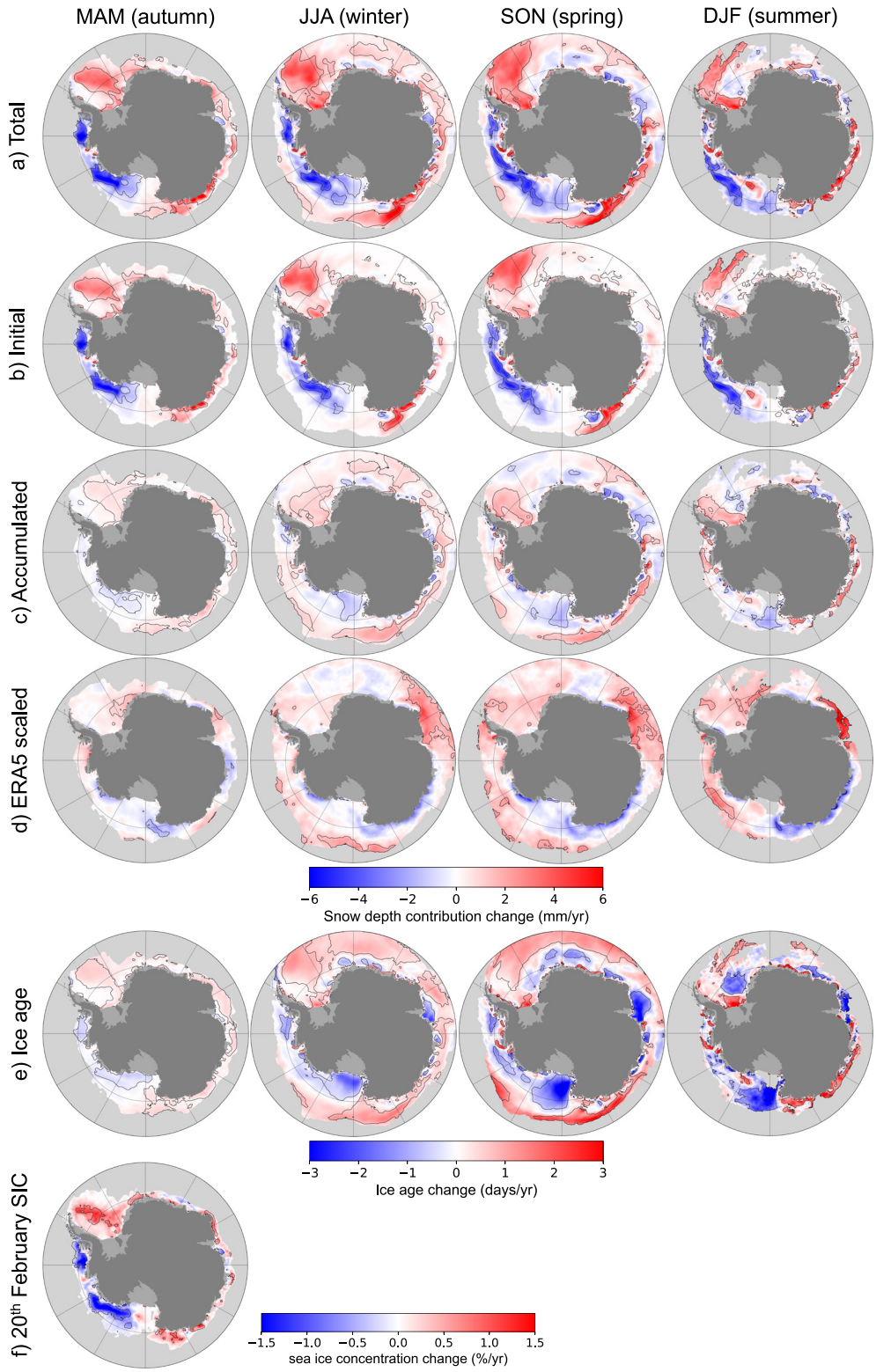

Figure 10. Trends in modeled sea ice snow depth and forcing between 1981 and 2021, calculated per season. Trend in (a) total snow depth (b) initial snow depth (c) accumulated snow depth (d) ERA5 snowfall, scaled by the percentage contribution of snowfall to snow depth after accounting for snow-ice formation and blown snow lost to the ocean (e) ice age, defined as the number of says a Lagrangian point is live (f) 20 February sea ice concentration. Black contours show regions where trends are significant ($P \leq 0.05$). A table of regional trends in seasonal and annual total snow depth is included in Supporting Information S1 (Table S1 in Supporting Information S1).

Bellingshausen, Amundsen or Ross seas from 2003 onwards in autumn, winter or spring), it is very likely that our model fails to capture regional trends relating to unique snow formation processes. Unfortunately, the lack of a temporally and spatially extensive in-situ data set precludes a validation of the trends.

Inaccurate representation of physical processes in the model would lead to a misinterpretation of the drivers. As explained above, the spatial pattern of trends in the initialization term results solely from the SIC on the 20 February. However, the magnitude of the initialization trends, and therefore their dominance over the total snow depth trends, are proportional to the magnitude of the snow depths we initialize with. Our model will therefore fail to capture any trend in snow depth relating to changes in the depth of the multi-year sea ice snow cover at the start of the growth season. Since we do not include any melt terms in the model, this trend analysis will also fail to capture any changes in the snow cover of Antarctic sea ice relating to trends in snow melt. Furthermore, trends in the prevalence of snow-ice production, which we keep fixed over the 41-year model duration, would have a significant effect on snow depth trends, as demonstrated by our sensitivity study (Section 3.2). It is notable however that trends in atmospheric snowfall, an expected key driver of trends in snow-ice production, are largely statistically insignificant over the model domain.

4. Discussion

4.1. Seasonal Growth of the Snow Cover

A key difference between the modeled and PM data sets is in the growth of the snow cover from winter to summer. Between winter and spring, CASSIS snow depths increase over both the SSM/I and AMSR periods (by ∼5 cm on average), while the SSM/I circumpolar average remains fixed between winter and spring (13.2 cm), with visible decrease in the snow cover of the West Weddell sector counterbalanced by minor increases (<1 cm) in Weddell East and Bellingshausen & Amundsen sectors (Figure S3 in Supporting Information S1). A lack of winter to spring snow growth in the SSM/I data was also found for the period 1979–2001 (Maksym & Markus, 2008), which the authors suggested could be due to all new snowfall being converted to snow-ice. This would be uncaptured in our model since we keep snow-ice formation fixed at 55%, and we note similarities in the pattern of positive CASSIS–SSM/I differences (Figure 7) and negative $CASSIS_{100}$–CASSIS differences (Figure 5) (note different scales), demonstrating that a switch to a 100% snow-ice regime in the model would produce spring snow depths more in line with those from SSM/I. However, for snow depth to remain constant by this mechanism requires that sea ice thickness also remains constant (assuming fixed snow and ice densities) (Maksym & Markus, 2008), and implies no correlation between snow depth and snow-ice thickness, which is not supported by field data (Massom et al., 2001). Therefore, we cannot rule out the possibility that the lack of a growth signal in the SSM/I data is an artefact, caused by changes in snow-pack morphology (e.g., grain size, snow wetness) which the PM methodology is sensitive to (Comiso et al., 2003; Markus & Cavalieri, 1998). On average, ASPeCt snow depth increases by 5 cm between winter and spring over the SSM/I period, increasing in every sector except the West Weddell, suggesting that the snow cover does thicken between these seasons. This could however be attributable to differences in spatial sampling. In general, CASSIS snow depths are too thick with respect to ASPeCt in spring, while SSM/I are too thin, which points to a combination of (a) CASSIS overestimating spring snow depth due an underestimation of snow-ice production, and (b) underestimated snow depth from SSM/I because of changes in snowpack properties that limit the PM methodology.

The increase in SSM/I snow depths between spring and summer (in all sectors and by 5 cm on average) is counter intuitive. If the lack of winter to spring growth was due to reaching a state of constant snow-ice production, then increased snow depths in summer would only result from a shift away from 100% snow-ice formation afforded by increasing ice thickness. Given that Southern Ocean sea ice melts predominantly from beneath in the summer due to high basal heat flux (Maksym et al., 2012), this seems implausible. If, on the other hand, the lack of growth signal was attributable to a change in snow-pack morphology, it is unclear why this would no longer be an issue in summer. The ASPeCt data also show a marked snow depth increase between spring and summer, though the difference in spatial sampling is apparent. In particular, we note that observations in the southern Amundsen Sea and Indian South East sector show very high snow depths (+40 cm). This could be explained by a sampling of the thicker snow near the coast in summer when the diminishing ice pack has allowed ships to get nearer the coast. This result does not necessarily mean therefore that snow depths on average increased between spring and summer. CASSIS, whose snow cover has decreased since the spring, shows a similar comparison to the ASPeCt data in summer as SSM/I does, though it is still an underestimate overall.

The same lack of a winter to spring signal is apparent in the AMSR data, with the circumpolar mean depth dropping from 12 to 11 cm, and decreasing or remaining constant in all sectors except the Bellingshausen & Amundsen which shows only a minor increase of 4 mm. There are even fewer ASPeCt data over the AMSR period with which to analyze the CASSIS and AMSR differences, including a complete absence of winter data outside of the Weddell Sea sectors, though the few winter samples that exist here agree on average more closely with CASSIS than AMSR. As before, spring snow depths are overestimated by CASSIS with respect to ASPeCt in the spring, but underestimated by PM (AMSR). This reinforces the idea that model snow depths are overestimated in the spring due to underestimated snow-ice formation, whilst being underestimated by PM. In a separate study comparing AMSR-E and ICESat estimates of snow depth between 2004 and 2006, ICESat was found to agree better with in-situ data from ASPeCt and OIB airborne data. Crucially, ICESat showed an increase of 7 cm in the mean snow cover between winter and spring, which was absent in the AMSR-E data, leading the authors to conclude that AMSR-E likely fails to capture the snow depth evolution due to sensitivity to changes in snow wetness and grain size (Kern & Ozsoy-çiçek, 2016). AMSR-E spring snow depths were also found to be significantly lower than in-situ from on-ice stations in the East Antarctic (Worby, Markus, et al., 2008), and 20–40 cm lower than ASPeCt over rough ice in the Bellingshausen Sea (Kern et al., 2011).

In contrast to SSM/I, summer snow depths from AMSR stay relatively constant, and are significantly lower than the ASPeCt observations in all sectors where data exist and by nearly 20 cm on average. As well as large discrepancies between AMSR and in-situ snow depths reported both here and in the cited literature, we find, for the period of overlap between 2003 and 2007, significant positive SSM/I–AMSR differences for all seasons, most notably in the summer where differences exceed 25 cm in places (Figure S5 in Supporting Information S1). We could find no mention of this lack of continuity of the PM data sets in the literature, which calls into question the validity of both.

4.2. ASPeCt Limitations

In our analysis we compare our results against ship-based estimates of snow depth from the ASPeCt data archive. It should be noted that these measurements are not strictly in-situ since they were recorded over the side of the moving ship rather than on the ground. The accuracy of recorded snow depths was estimated, by comparison with drill-hole measurements, as 20% for snow thicker than 30 cm, increasing to 50% for snow less than 10 cm thick (Worby, Geiger, et al., 2008). However, since these errors are independent from one measurement to the next, we expect they reduce when we calculate segment-average snow depths for our analysis. Worby, Geiger, et al. (2008) also highlight that snow depth is only recorded over level ice and therefore the data archive excludes the thicker snow found at ridges. This omission is likely to improve both our model validation, since we do not account for convergence and ridging in the model, and the comparison to PM retrievals which work best for level ice (Comiso et al., 2003; Markus & Cavalieri, 1998). As well as selective recording over level ice, ships will preferentially traverse thin, lead-rich ice, thereby sampling the lower end of the sea ice thickness distribution which has a thinner snow layer (Worby, Geiger, et al., 2008). This is evident from autumn to spring by the lack of ASPeCt measurements over the thickest snow near the coast, and explains the increase in ASPeCt data in these regions in the summer as the ice pack melts and breaks up, allowing ships to enter more easily. As highlighted in the previous section, spatial sampling differences make assessing the seasonal evolution of the ASPeCt snow cover difficult, as well as the performance of CASSIS and PM in one season versus another. Although the ASPeCt data are far from perfect, they are the only spatially and temporally extensive observational data set of snow depth on Southern Ocean sea ice and we are therefore reliant on them for calibration and validation of remotely sensed and modeled data sets.

4.3. Model Limitations

The comparison to ASPeCt data (Figure S1 in Supporting Information S1) suggests that we initialize CASSIS with too-thin a snow layer in the Weddell West sector and the western Amundsen/eastern Ross Sea. Comparison to data from OIB (Section 3.3.2) also highlights that we likely underestimate snow depth over deformed ice due to lack of ice/snow convergence processes in the model. This could also explain the differences between CASSIS and ASPeCt in the summer, which are dominated by results from four ship tracks; two in the Amundsen Sea, one off the coast of the western Weddell Sea, and one near the coast of the Indian South East sector. Along these tracks, ships encounter thick snow depths, often in excess of 50 cm, which CASSIS does not reproduce. However,

given that ASPeCt is supposed to represent the snow depth over level (undeformed) ice, the thick snow depths reported could also be attributed to wind redistribution. Although we account for deposition of snow blown off the Antarctic continent by strong winds, our model does not include redistribution of snow by winds (other than lost to ocean). It has been previously reported that Katabatic winds can strip the ice near the coast of snow and redeposit it some tens to hundreds of kilometers offshore (Bromwich & Kurtz, 1984). It is plausible that ships traversed and sampled these regions of thick, redistributed snow, resulting in inconsistency between ASPeCt and CASSIS in these cases.

We find that, compared to ASPeCt data, model spring snow depths are overestimated, which could be attributable to increased snow-ice production in the spring (Massom et al., 2001) which is not reproduced in CASSIS. In our sensitivity study, we find that our fixed ratio of snow-to-snow-ice conversion imposes an uncertainty on CASSIS season-average snow depths of up to ±40 cm in some regions. At present, observations of snow-ice thickness are too temporally and spatially limited to build a seasonally and regionally -dependent model parametrization. Dedicated field campaigns to monitor the seasonal evolution of the snow-ice layer in different sectors of the Southern Ocean are required.

Spring snow depths may also be overestimated because the model does not include any melt terms. Surface melt is less common in Antarctica than the Arctic; melt ponds have rarely been reported on the snow surface and ice that survives the melt season typically retains its snow cover (Massom et al., 2001; Webster et al., 2018). Although Snow Buoys have revealed some surface melting of the summer snowpack, only a few buoys in the marginal ice zone experienced strong surface ablation, and complete melt or evaporation of the snow cover was not observed (Nicolaus et al., 2021). However superimposed ice resulting from the trickling down and refreezing of melt water in the snowpack of perennial ice has been widely reported in summer (Arndt, 2022; Haas et al., 2001; Massom et al., 2001), resulting in a reduction of the snow cover. As discussed in Section 2.3, the blowing snow loss term, since its magnitude is calibrated to the in-situ data, will also incorporate snow loss due to other factors like snow melt. That is, if the model included a snow melt term which reduced the snow cover in spring and summer, the blowing snow term, once recalibrated, would remove less snow such that the comparison of snow depth to the in-situ data was approximately equivalent. A future iteration of the model should include separate snow-ice, blowing snow, and snow melt terms, each a function of the environmental factors which drive them and calibrated in parallel. For this version of the data set the snow-ice and blowing-snow loss terms combine to reduce the snow cover to something with realistic spatial distribution and reasonable comparison to the in-situ data, even though the proportions removed by each are uncertain and the combined loss also incorporates melt. The fact that ASPeCt snow depths are larger than CASSIS in summer reinforces the idea that surface melt has been accounted for in the simulations, albeit not directly.

The fixed snow-ice parametrization and lack of a snow melt term will also impact our trend analysis, and we re-emphasize that the conclusions of the trend analysis are a model result. We find however that the dominant 1981–2021 trend signal results from changes in summer SIC (or more specifically, 20 February sea ice extent), which could be considered largely independent of snow-ice formation and snow melt. Our results are supported by Maksym and Markus (2008), who found small but significant positive trends in snow depth from AMSR-E between 1979 and 2001 in all regions except the Bellingshausen & Amundsen, where snow depth decreased. Like us, they attribute trends primarily to the timing of the sea ice season. A trend analysis over the full duration of the PM record could be beneficial, but problems with retrievals over rough ice as well as the discontinuity between SSM/I and AMSR must be addressed first.

5. Conclusions

Snow on sea ice is an important component of the mass budget of the Southern Ocean, and knowing its depth and density is essential for deriving sea ice thickness and volume from satellite altimetry. Recently emerging snow depth products utilizing dual satellite altimetry are reliant on the assumption that Ku-band radar fully penetrates the snow cover, which is not supported by field studies. Furthermore, these multi-satellite products cannot complement the complete record of altimetry data acquired over Antarctic sea ice since the launch of ERS-1 in 1991. Snow depth estimates spanning multiple decades are available from PM satellite data, but the method is sensitive to snow melt and grain size, and can only resolve snow depths up to 50 cm. Therefore, a snow depth product that is not limited by these issues and which spans the full altimetry record is desirable for the sea ice community.

Here we present the CPOM Antarctic Snow on Sea Ice Simulation, CASSIS, a Lagrangian-network snow accumulation model forced with atmospheric reanalysis, satellite-derived SIC and sea ice motion. The model is initialized with a regionally-variable snow depth each year at the start of the growth season. Sources of snow accumulation are atmospheric snowfall and snow blown off the Antarctic continent by Katabatic winds, though the latter has a negligible contribution. A portion of the accumulated snow is blown into the ocean, after which 55% of the remaining daily accumulated snow layer is lost to snow-ice formation.

Snow depths from the model compare reasonably well with in-situ data from ships (mean difference = 1.9 cm, RMSD = 13.1 cm) and OIB aircraft surveys (mean difference = 7.3 cm, RSMD = 13.5). Differences likely result from both model limitations and uncertainties in the validation data. A detailed comparison to ship data suggests we may initialize the model with too-thin a snow cover in some regions, and that snow-ice formation is underestimated in the spring. A sensitivity study exploring the impact of the fixed snow-ice conversion term reveals errors of ±40 cm in some regions. Despite its drawbacks, our model offers an alternative multi-decadal snow depth solution to those from PM, which fail to capture the seasonal evolution of the snow cover. We emphasize the need for dedicated field studies to assess the regional and seasonal variability of snow-ice formation, and conduct a more comprehensive comparison/validation of the different snow products.

An analysis of the 40-year trends in the snow cover of Antarctic sea ice reveal that although the thickness of the circumpolar snow cover has increased overall, snow depth has decreased in the South Pacific owing to reduced late-summer SIC in this region.

CASSIS snow depths could complement decades of satellite altimetry data to provide new-and-improved estimates of sea ice thickness and progress understanding of Antarctic sea ice variability.

Conflict of Interest

The authors declare no conflicts of interest relevant to this study.

Data Availability Statement

The ship-based snow thickness data 1981–2016 data were provided by the SCAR Antarctic Sea Ice Processes and Climate (ASPeCt) program. The original ASPeCt data set for the Southern Hemisphere 1980–2005 were downloaded from the ASPeCt website at aspect.antarctica.gov.au/data.html (ASPeCt Data, 2012). The more recent data (2002–2019) were downloaded from the World Data Center for Climate (WDCC) at DKRZ via doi.org/10.26050/WDCC/ESACCIPSMVSBSIO (Kern, 2020). ERA5 atmospheric reanalysis data used as input for the model are available from the Copernicus Climate Change Service (C3S) Climate Data Store (CDS) via doi.org/10.24381/cds.adbb2d47 (Hersbach et al., 2023). Sea ice concentration and sea ice motion data used to drive the model are available from the NSIDC via doi.org/10.5067/8GQ8LZQVL0VL (Cavalieri et al., 1996) and doi.org/10.5067/INAWUWO7QH7B (Tschudi et al., 2019). For estimating snow blown onto sea ice from the Antarctic continent we used data from the regional atmospheric climate model RACMO2.3, version p1, archived on PANGAEA via doi.org/10.1594/PANGAEA.896940 (van den Broeke, 2019). SSM/I snow depths were downloaded from NASA GSFC: earth.gsfc.nasa.gov/cryo/data/antarctic-snow-depth-sea-ice (NASA, 2023), and AMSR-E and AMSR2 snow depths estimates are archived at the NSIDC via doi.org/10.5067/AMSR-E/AE_SI12.003 (Cavalieri et al., 2014) and doi.org/10.5067/RA1MIJOYPK3P (Meier et al., 2018). CASSIS snow model data are available at: cpom.ucl.ac.uk/cassis (CPOM, 2023).

Acknowledgments
This work was supported predominantly by the Natural Environment Research Council (NERC) through National Capability funding, undertaken by a partnership between the Centre for Polar Observation and Modelling and the British Antarctic Survey, and by the NERC DEFIANT project, Grant NE/W004747/1. IRL acknowledges support from the European Space Agency during revisions and final preparation of the manuscript. We would like to thank Michiel van den Broeke for assisting in developing the katabatic snow parameter. Extended thanks also to our three reviewers for their thorough evaluation of our paper.

References

Adolphs, U., & Wendler, G. (1995). A pilot study on the interactions between katabatic winds and polynyas at the Adblie Coast, eastern Antarctica. *Antarctic Science*, *7*(3), 307–314. https://doi.org/10.1017/S0954102095000423

Andreas, E. L. (1995). Air-ice drag coefficients in the western Weddell Sea 2. A model based on form drag and drifting snow. *Journal of Geophysical Research*, *100*(C3), 4833–4843. https://doi.org/10.1029/94JC02016

Arndt, S. (2022). Sensitivity of sea ice growth to snow properties in opposing regions of the Weddell Sea in late summer. *Geophysical Research Letters*, *49*(19), e2022GL099653. https://doi.org/10.1029/2022GL099653

ASPeCt Data. (2012). Retrieved from https://aspect.antarctica.gov.au/data.html

Blanchard-Wrigglesworth, E., Webster, M. A., Farrell, S. L., & Bitz, C. M. (2018). Reconstruction of snow on Arctic Sea ice. *Journal of Geophysical Research: Oceans*, *123*(5), 3588–3602. https://doi.org/10.1002/2017JC013364

Boisvert, L. N., Webster, M. A., Petty, A. A., Markus, T., Cullather, R. I., & Bromwich, D. H. (2020). Intercomparison of precipitation estimates over the southern ocean from atmospheric reanalyses. *Journal of Climate*, *33*(24), 10627–10651. https://doi.org/10.1175/JCLI-D-20-0044.1

Bromwich, D. H., & Kurtz, D. D. (1984). Katabatic wind forcing of the Terra Nova Bay Polynya. *Journal of Geophysical Research*, *89*(4), 3561–3572. https://doi.org/10.1029/jc089ic03p03561

Cavalieri, D. J., Markus, T., & Comiso, J. C. (2014). *AMSR-E/Aqua daily L3 12.5 km brightness temperature, sea ice concentration, & snow depth polar grids, Version 3. [subset]*. NASA National Snow and Ice Data Center Distributed Active Archive Center. https://doi.org/10.5067/AMSR-E/AE_SI12.003

Cavalieri, D. J., Parkinson, C. L., Gloersen, P., & Zwally, H. J. (1996). *Sea ice concentrations from Nimbus-7 SMMR and DMSP SSM/I-SSMIS passive microwave data, Version 1*. NASA National Snow and Ice Data Center Distributed Active Archive Center. (p. Updated yearly). https://doi.org/10.5067/8GQ8LZQVL0VL

Comiso, J. C., Cavalieri, D. J., & Markus, T. (2003). Sea ice concentration, ice temperature, and snow depth using AMSR-E data. *IEEE Transactions on Geoscience and Remote Sensing*, *41*(2 PART 1), 243–252. https://doi.org/10.1109/TGRS.2002.808317

CPOM. (2023). CASSIS - Snow depth data. Retrieved from http://www.cpom.ucl.ac.uk/cassis/

Dai, L., Xie, H., Ackley, S. F., & Mestas-Nuñez, A. M. (2020). Ice production in Ross Ice Shelf polynyas during 2017–2018 from sentinel-1 SAR images. *Remote Sensing*, *12*(9), 18–26. https://doi.org/10.3390/RS12091484

Dong, X., Wang, Y., Shugui, H. O. U., Ding, M., Baoling, Y. I. N., & Zhang, Y. (2020). Robustness of the recent global atmospheric reanalyses for Antarctic near-surface wind speed climatology. *Journal of Climate*, *33*(10), 4027–4043. https://doi.org/10.1175/JCLI-D-19-0648.1

Eayrs, C., Li, X., Raphael, M. N., & Holland, D. M. (2021). Rapid decline in Antarctic sea ice in recent years hints at future change. *Nature Geoscience*, *14*(July), 10–14. https://doi.org/10.1038/s41561-021-00768-3

Eicken, H., Lange, M. A., Hubberten, H.-W., & Wadhams, P. (1994). Characteristics and distribution patterns of snow and meteoric ice in the Weddel Sea and their contribution to the mass balance of sea ice. *Annales Geophysicae*, *12*(1), 80–93. https://doi.org/10.1007/s00585-994-0080-x

Fedotov, V. I., Cherepanov, N. V., & Tyshko, K. P. (1998). Some features of the growth, structure and metamorphism of east Antarctic landfast sea ice. *Antarctic Research Series*, *74*, 343–354.

Fichefet, T., & Maqueda, M. (1999). Modelling the influence of snow accumulation and snow-ice formation on the seasonal cycle of the Antarctic sea-ice cover. *Climate Dynamics*, *15*(4), 251–268. https://doi.org/10.1007/s003820050280

Fons, S. W., Kurtz, N. T., Bagnardi, M., Petty, A. A., Tilling, R. L., & Fons, S. W. (2021). Assessing CryoSat-2 Antarctic snow freeboard retrievals using data from ICESat-2 1. *Earth and Space Science*, *2*, 1–17. https://doi.org/10.1029/2021EA001728

Garnier, F., Fleury, S., Garric, G., Bouffard, J., Tsamados, M., Laforge, A., et al. (2021). Advances in altimetric snow depth estimates using bi-frequency SARAL and CryoSat-2 Ka-Ku measurements. *The Cryosphere*, *15*(12), 5483–5512. https://doi.org/10.5194/tc-15-5483-2021

Giles, K. A., Laxon, S. W., Wingham, D. J., Wallis, D. W., Krabill, W. B., Leuschen, C. J., et al. (2007). Combined airborne laser and radar altimeter measurements over the Fram Strait in May 2002. *Remote Sensing of Environment*, *111*(2), 182–194. https://doi.org/10.1016/j.rse.2007.02.037

Giles, K. A., Laxon, S. W., & Worby, A. P. (2008). Antarctic sea ice elevation from satellite radar altimetry. *Geophysical Research Letters*, *35*(3), L03503. https://doi.org/10.1029/2007GL031572

Gossart, A., Helsen, S., Lenaerts, J. T. M., Vanden Broucke, S., van Lipzig, N. P. M., & Souverijns, N. (2019). An evaluation of surface climatology in state-of-the-art reanalyses over the Antarctic Ice Sheet. *Journal of Climate*, *32*(20), 6899–6915. https://doi.org/10.1175/JCLI-D-19-0030.1

Guerreiro, K., Fleury, S., Zakharova, E., Rémy, F., & Kouraev, A. (2016). Potential for estimation of snow depth on Arctic sea ice from CryoSat-2 and SARAL/AltiKa missions. *Remote Sensing of Environment*, *186*, 339–349. https://doi.org/10.1016/j.rse.2016.07.013

Haas, C., Thomas, D. N., & Bareiss, J. (2001). Surface properties and processes of perennial Antarctic sea ice in summer. *Journal of Glaciology*, *47*(159), 613–625. https://doi.org/10.3189/172756501781831864

Hersbach, H., Bell, B., Berrisford, P., Biavati, G., Horányi, A., Muñoz Sabater, J., et al. (2023). *ERA5 hourly data on single levels from 1940 to present*. Copernicus Climate Change Service (C3S) Climate Data Store (CDS). https://doi.org/10.24381/cds.adbb2d47

Holland, M. M., Clemens-Sewall, D., Landrum, L., Light, B., Perovich, D., Polashenski, C., et al. (2021). The influence of snow on sea ice as assessed from simulations of CESM2. *The Cryosphere*, *15*(10), 4981–4998. https://doi.org/10.5194/tc-15-4981-2021

Huang, Y., Siems, S. T., Manton, M. J., Rosenfeld, D., Marchand, R., McFarquhar, G. M., & Protat, A. (2016). What is the role of sea surface temperature in modulating cloud and precipitation properties over the Southern Ocean? *Journal of Climate*, *29*(20), 7453–7476. https://doi.org/10.1175/JCLI-D-15-0768.1

Jeffries, M. O., Krouse, H. R., Hurst-Cushing, B., & Maksym, T. (2001). Snow-ice accretion and snow-cover depletion on Antartic first-year sea-ice floes. *Annals of Glaciology*, *33*, 51–60. https://doi.org/10.3189/172756401781818266

Jeffries, M. O., Veazey, A. L., Morris, K., & Krouse, H. R. (1994). Depositional environment of the snow cover on West Antarctic pack-ice floes. *Annals of Glaciology*, *20*, 33–38. https://doi.org/10.3189/1994aog20-1-33-38

Kacimi, S., & Kwok, R. (2020). The Antarctic sea ice cover from ICESat-2 and CryoSat-2: Freeboard, snow depth and ice thickness. *The Cryosphere*, *14*, 4453–4474. https://doi.org/10.5194/tc-2020-145

Kacimi, S., & Kwok, R. (2022). Arctic snow depth, ice thickness, and volume from ICESat-2 and CryoSat-2: 2018–2021. *Geophysical Research Letters*, *49*(5), e2021GL097448. https://doi.org/10.1029/2021GL097448

Kern, S. (2009). Wintertime Antarctic coastal polynya area: 1992–2008. *Geophysical Research Letters*, *36*(14), 1–5. https://doi.org/10.1029/2009GL038062

Kern, S. (2020). *ESA-CCI_Phase2_Standardized_Manual_Visual_Ship-Based_SeaIceObservations_v02*. Integrated Climate Data Center (ICDC) at CEN, University of Hamburg, and World Data Center for Climate (WDCC) at DKRZ. https://doi.org/10.26050/WDCC/ESACCIPSMVSBSIOV2

Kern, S., & Ozsoy-çiçek, B. (2016). Satellite remote sensing of snow depth on Antarctic Sea Ice: An inter-comparison of two empirical approaches. *Remote Sensing*, *8*(6), 450. https://doi.org/10.3390/rs8060450

Kern, S., Ozsoy-cicek, B., Willmes, S., Nicolaus, M., Haas, C., & Ackley, S. (2011). An intercomparison between AMSR-E snow-depth and satellite C- and Ku-band radar backscatter data for Antarctic sea ice. *Annals of Glaciology*, *52*(57), 279–290. https://doi.org/10.3189/172756411795931750

Kurtz, N. T., & Markus, T. (2012). Satellite observations of Antarctic sea ice thickness and volume. *Journal of Geophysical Research*, *117*(8), C08025. https://doi.org/10.1029/2012JC008141

Kwok, R., & Maksym, T. (2014). Snow depth of the Weddell and Bellingshausen sea ice covers from IceBridge surveys in 2010 and 2011: An examination. *Journal of Geophysical Research: Oceans*, *119*(7), 4141–4167. https://doi.org/10.1002/2017JC013159

Lawrence, I. R., Tsamados, M. C., Stroeve, J. C., Armitage, T. W. K., & Ridout, A. L. (2018). Estimating snow depth over Arctic sea ice from calibrated dual-frequency radar freeboards. *The Cryosphere*, *12*(11), 3551–3564. https://doi.org/10.5194/tc-12-3551-2018

Liston, G. E., Itkin, P., Stroeve, J., Tschudi, M., Stewart, J. S., Pedersen, S. H., et al. (2020). A Lagrangian snow-evolution system for sea-ice applications (SnowModel-LG): Part I—Model description. *Journal of Geophysical Research: Oceans*, *125*(10), e2019JC015913. https://doi.org/10.1029/2019JC015913

Lytle, V. I., & Ackley, S. F. (2001). Snow-ice growth: A fresh-water flux inhibiting deep convection in the Weddell Sea, Antartica. *Annals of Glaciology*, *33*, 45–50. https://doi.org/10.3189/172756401781818752

Maksym, T. (2019). Arctic and Antarctic sea ice change: Contrasts, commonalities, and causes. *Annual Review of Marine Science*, *11*(1), 187–213. https://doi.org/10.1146/annurev-marine-010816-060610

Maksym, T., & Markus, T. (2008). Antarctic sea ice thickness and snow-to-ice conversion from atmospheric reanalysis and passive microwave snow depth. *Journal of Geophysical Research*, *113*(C2), C02S12. https://doi.org/10.1029/2006JC004085

Maksym, T., Stammerjohn, S. E., Ackley, S., & Massom, R. (2012). Antarctic sea ice — A polar opposite? *Oceanography*, *25*(3), 140–151. Special issue on Antarctic oceanography in a changing world. https://doi.org/10.5670/oceanog.2012.88

Markus, T., & Cavalieri, D. J. (1998). Snow depth distribution over sea ice in the Southern Ocean from satellite passive microwave data. *Antarctic Research Series*, *74*, 19–39. https://doi.org/10.1029/AR074p0019

Massom, R. A., Eicken, H., Haas, C., Jeffries, M. O., Drinkwater, M. R., Sturm, M., et al. (2001). Snow on Antarctic sea ice. *Reviews of Geophysics*, *39*(3), 413–445. https://doi.org/10.1029/2000rg000085

Meier, W. N., Markus, T., & Comiso, J. C. (2018). *AMSR-E/AMSR2 unified L3 daily 12.5 km brightness temperatures, sea ice concentration, motion & snow depth polar grids, Version 1 [subset]*. NASA National Snow and Ice Data Center Distributed Active Archive Center. https://doi.org/10.5067/RA1MIJOYPK3P

Merkouriadi, I., Cheng, B., Graham, R. M., Rösel, A., & Granskog, M. A. (2017). Critical role of snow on sea ice growth in the Atlantic sector of the Arctic Ocean. *Geophysical Research Letters*, *44*(20), 10479–10485. https://doi.org/10.1002/2017GL075494

NASA. (2023). Antarctic snow depth on sea ice. Retrieved from https://earth.gsfc.nasa.gov/cryo/data/antarctic-snow-depth-sea-ice

Nicolaus, M., Arndt, S., Hendricks, S., Heygster, G., Huntemann, M., Katlein, C., et al. (2016). *Snow depth on Arctic and Antarctic sea ice derived from snow buoys*. General Assembly of the European Geosciences Union.

Nicolaus, M., Hoppmann, M., Arndt, S., Hendricks, S., Katlein, C., Nicolaus, A., et al. (2021). Snow depth and air temperature seasonality on sea ice derived from snow buoy measurements. *Frontiers in Marine Science*, *8*(April), 1–21. https://doi.org/10.3389/fmars.2021.655446

NSIDC. (2003). Sea ice concentrations from Nimbus-7 SMMR and DMSP SSM/I passive microwave data, Version 1, User Guide. Retrieved from https://nsidc.org/data/nsidc-0051/versions/1

NSIDC. (2021). Sea ice tools. Retrieved from https://nsidc.org/arcticseaicenews/sea-ice-tools/

Petty, A. A., Webster, M., Boisvert, L., & Markus, T. (2018). The NASA Eulerian Snow on Sea Ice Model (NESOSIM) v1.0: Initial model development and analysis. *Geoscientific Model Development*, *11*, 4577–4602. https://doi.org/10.5194/gmd-11-4577-2018

Powell, D. C., Markus, T., & Stössel, A. (2005). Effects of snow depth forcing on Southern Ocean sea ice simulations. *Journal of Geophysical Research*, *110*(6), 1–10. https://doi.org/10.1029/2003JC002212

Sodemann, H., & Stohl, A. (2009). Asymmetries in the moisture origin of Antarctic precipitation. *Geophysical Research Letters*, *36*(22), 1–5. https://doi.org/10.1029/2009GL040242

Sturm, M., Morris, K., & Massom, R. (1998). The winter snow cover of the west Antarctic pack ice: Its spatial and temporal variability. *Antarctic Research Series*, *74*, 1–18.

Tamura, T., Ohshima, K. I., & Nihashi, S. (2008). Mapping of sea ice production for Antarctic coastal polynyas. *Geophysical Research Letters*, *35*(7), 1–5. https://doi.org/10.1029/2007GL032903

Tschudi, M., Meier, W. N., & Scott Stewart, J. (2020). An enhancement to sea ice motion and age products at the National Snow and Ice Data Center (NSIDC). *The Cryosphere*, *14*(5), 1519–1536. https://doi.org/10.5194/tc-14-1519-2020

Tschudi, M., Meier, W. N., Stewart, J. S., Fowler, C., & Maslanik, J. (2019). *Polar pathfinder daily 25 km EASE-grid sea ice motion vectors, Version 4*. NASA National Snow and Ice Data Center Distributed Active Archive Center. https://doi.org/10.5067/INAWUWO7QH7B

Turner, J., Guarino, M. V., Arnatt, J., Jena, B., Marshall, G. J., Phillips, T., et al. (2020). Recent decrease of summer sea ice in the Weddell Sea, Antarctica. *Geophysical Research Letters*, *47*(11), e2020GL087127. https://doi.org/10.1029/2020GL087127

van den Broeke, M. R. (2019). RACMO2.3p1 annual surface mass balance Antarctica (1979–2014). *PANGAEA*. https://doi.org/10.1594/PANGAEA.896940

van Wessem, J. M., van de Berg, W. J., Noël, B. P. Y., van Meijgaard, E., Amory, C., Birnbaum, G., et al. (2018). Modelling the climate and surface mass balance of polar ice sheets using RACMO2 - Part 2: Antarctica (1979-2016). *The Cryosphere*, *12*(4), 1479–1498. https://doi.org/10.5194/tc-12-1479-2018

Wang, Z., Turner, J., Wu, Y., & Liu, C. (2019). Rapid decline of total Antarctic sea ice extent during 2014 – 16 controlled by wind-driven sea ice drift. *Journal of Climate*, *32*(17), 5381–5395. https://doi.org/10.1175/JCLI-D-18-0635.1

Webster, M., Gerland, S., Holland, M., Hunke, E., Kwok, R., Lecomte, O., et al. (2018). Snow in the changing sea-ice systems. *Nature Climate Change*, *8*(11), 946–952. https://doi.org/10.1038/s41558-018-0286-7

Wever, N., Leonard, K., Maksym, T., White, S., Proksch, M., & Lenaerts, J. T. M. (2021). Spatially distributed simulations of the effect of snow on mass balance and flooding of Antarctic sea ice. *Journal of Glaciology*, *67*(266), 1055–1073. https://doi.org/10.1017/jog.2021.54

Willatt, R. C., Giles, K. A., Laxon, S. W., Stone-Drake, L., & Worby, A. P. (2010). Field investigations of Ku-band radar penetration into snow cover on Antarctic sea ice. *IEEE Transactions on Geoscience and Remote Sensing*, *48*(1), 365–372. https://doi.org/10.1109/TGRS.2009.2028237

Worby, A. P., Geiger, C. A., Paget, M. J., Van Woert, M. L., Ackley, S. F., & DeLiberty, T. L. (2008). Thickness distribution of Antarctic sea ice. *Journal of Geophysical Research*, *113*(5), 1–14. https://doi.org/10.1029/2007JC004254

Worby, A. P., Markus, T., Steer, A. D., Lytle, V. I., & Massom, R. A. (2008). Evaluation of AMSR-E snow depth product over East Antarctic sea ice using in situ measurements and aerial photography. *Journal of Geophysical Research*, *113*(C5), C05S94. https://doi.org/10.1029/2007JC004181